Inorganic Chemistry

pubs.acs.org/IC

Article

Cytotoxic Ruthenium(II) Complexes Containing a Dangling Pyridine: Selectivity for Diseased Cells Mediated by pH-Dependent DNA Binding

Somasundaram Sangeetha and Mariappan Murali*

Cite This: *Inorg. Chem.* 2022, 61, 2864−2882

Read Online

ACCESS | Metrics & More | Article Recommendations | Supporting Information

ABSTRACT: Ruthenium(II) complexes of the type $[Ru(bpy)_2(L^1/L^2/L^3)]PF_6$ [where bpy = 2,2′-bipyridine, $H(L^1)$ = *N*-(pyrid-2-yl)salicylaldimine (**1**), $H(L^2)$ = *N*-(6-methylpyrid-2-yl)salicylaldimine (**2**), and $H(L^3)$ = *N*-(4,6-dimethylpyrid-2-yl)salicylaldimine (**3**)] have been isolated. The X-ray structures of **1**−**3** reveal distorted octahedral coordination geometry with a planar ruthenium phenolate moiety. They exhibit interpair dimeric association in their solid state such as (a) $\pi-\pi$-stacking interactions (**1**−**3**) and (b) C−H···π interactions (**2**). The ^{1}H NMR spectral data shed light on the characteristics of metal−ligand bonding and chelate ring conformations. The complexes exhibit strong metal-to-ligand charge-transfer transitions in the visible region. The complexes also undergo two successive metal-based oxidative processes corresponding to the Ru^{II}/Ru^{III} and Ru^{III}/Ru^{IV} couples. Resonance Raman studies strongly suggest that the lowest unoccupied molecular orbital of **1**−**3** is localized at the bpy ligand. Absorption, emission, and circular dichroic spectral measurements for **1**−**3** with calf-thymus DNA reveal a groove binding mode of interaction. Interestingly, all of the complexes exhibit pH-dependent DNA damage, and the pH at which the damage is highest corresponds to the pH conditions of the cancer cells. The DNA damage is in the order of **3** > **2** > **1**, in which a hydrolytic mechanism dominates. The protein binding properties of the complexes examined by the tryptophan quenching measurements suggest a static mechanism. The positive ΔH and ΔS values indicate that the force acting between the complexes and bovine serum albumin (BSA) is mainly a hydrophobic interaction, and thus BSA may act as a targeted drug-delivery vehicle for ruthenium(II) complexes ($K \sim 10^5$). It is noteworthy that **3** exhibits selectivity with high cytotoxicity against breast cancer cells (EVSA-T and MCF-7), and its potency is comparable to that of cisplatin.

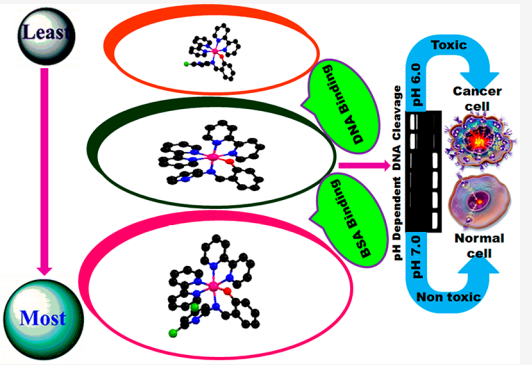

INTRODUCTION

Cisplatin is one of the most extensively used antitumor drugs to treat many cancers.[1] It causes cytotoxicity by cross-linking DNA, inducing alterations in the DNA structure that prevent replication and protein synthesis. However, high general toxicity, severe side effects, and increasing drug resistance have restricted the clinical application of cisplatin. The introduction of special drug-dosing protocols[2] has lowered the general toxicity of cisplatin, although there is still a scope for further improvements. This gives the thrust to explore metallodrugs bearing metal ions other than platinum. Under physiological conditions, the oxidation states Ru^{II}, Ru^{III}, and Ru^{IV} are all accessible to ruthenium, making it unique among the platinum group metals. Ruthenium(III) complexes tend to be more biologically inert than related ruthenium(II) and ruthenium(IV) complexes. Ruthenium-based anticancer drugs[3] show low general toxicity and demonstrate remarkable anticancer activity compared to platinum compounds and accumulate particularly in cancer cells.[4] The capacity of ruthenium to mimic iron ion binding to particular proteins, such as serum transferrin and albumin, which are known to be responsible for the solubilization, transport, and detoxification of iron in mammals, explains the decreased toxicity.[4] Rapidly proliferating cancer cells have a higher demand for iron, resulting in an overexpression of transferrin receptors on their surfaces, causing ruthenium compounds to accumulate in the cells.[4]

The discovery of two interesting ruthenium(III) coordination compounds, (ImH)*trans*-$[Ru^{III}Cl_4(DMSO)(Im)]$ (NAMI-A; Im = imidazole and DMSO = dimethyl sulfoxide)[5] and (IndH)*trans*-$[Ru^{III}Cl_4(Ind)_2]$ (KP1019; Ind = indazole),[6] developed by the groups of Alessio and Keppler, respectively, was the first breakthrough in the field of ruthenium-based

Received: October 31, 2021
Published: January 31, 2022

https://doi.org/10.1021/acs.inorgchem.1c03399
Inorg. Chem. 2022, 61, 2864−2882

Scheme 1. Structure and Proton Numbering Scheme of Ligands

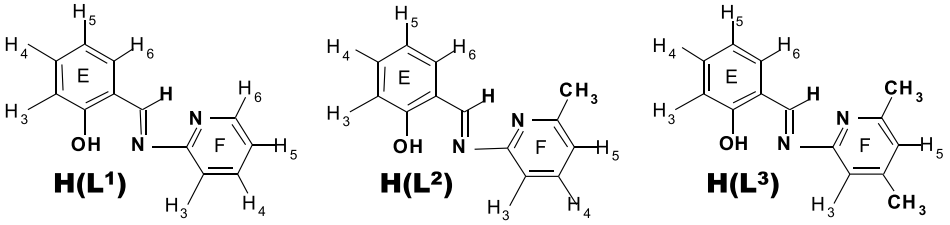

anticancer drug prospects. Despite the various studies conducted to date, the mechanisms of action of NAMI-A and KP-1019 remain mostly unclear. Alessio described a variety of unproven myths that have grown up around the NAMI-A and KP-1019 compounds over the years, significantly impacting the entire field of ruthenium anticancer drugs.[7] Rather, these substances have significantly boosted interest in nonplatinum anticancer metal compounds and broadened the logical approach to this field. The principal molecular target of metal-based anticancer drugs like cisplatin has been identified as DNA.[8−10] So, the interaction of ruthenium complexes with DNA is being studied to see if DNA binding is effective and if they may be employed as chemotherapeutic drugs. The ruthenium(III) complexes are thought to have a different mode of action than platinum(II) drugs. These ruthenium(III) complexes are reduced to reactive ruthenium(II) species in hypoxic tumor tissues and form DNA adducts, adding to the cytostatic effects. As a result, the development of ruthenium-(II) anticancer complexes that have both substantial solubility in aqueous solutions and cell uptake has received a lot of interest in the field of biocoordination chemistry to circumvent the reduction step.[11] New classes of cationic and neutral half-sandwich ruthenium(II) arene compounds (also known as piano-stool compounds) discovered by the Sadler {[(η^6-biphenyl)Ru(en)Cl](PF$_6$) (RM175; en = ethane-1,2-diamine)} and Dyson {[(η^6-*p*-cymene)RuCl$_2$(pta)] (RAPTA-C; pta = 1,3,5-triaza-7-phosphatricyclo[3.3.1.1]-decane)}[12,13] groups in recent years have been revealed to have promise anticancer action *in vivo* and *in vitro*. All of the ruthenium-based drugs have developed with the intent of covalently binding the metallic center to its destination (DNA). Noncovalent interactions between DNA and other molecules are common in nature and have a significant impact. It can be demonstrated in the realms of recognition[14] and antibiotics[15] and useful in the development of new drugs. Groove binding (major and minor) and intercalation[16] are the two main types of noncovalent DNA bindings that have been recognized for the last 60 years. Metallodrugs that bind noncovalently to DNA in these two ways have been developed and have different actions to cisplatin.[16] Intercalation appreciably influences the DNA characteristics and is described as an early step in mutagenesis.[17] In particular, metal complexes with planar aromatic ligands that intercalate to DNA are gaining a great deal of current research.[18] These metallointercalators are highly mutagenic, and some have demonstrated potential chemotherapeutic efficacy, which is based on their propensity for DNA binding.[19] Moreover, complexes with properly oriented hydrogen-bonding capabilities can effectively bind to DNA in either the major or minor grooves.[20]

Serum albumin (SA) in blood plasma is the most prevalent soluble protein.[21] It is involved in the transportation, distribution, and metabolism of a wide range of exogenous and endogenous compounds, including metal ions, fatty acids, amino acids, and drugs.[22,23] Generally, a medicinal drug with SA is transported and distributed in four steps:[24] (i) the drug is transferred across a biological membrane from its original binding site or plate; (ii) the drug interacts with SA under equilibrium conditions to form a drug−SA complex; (iii) the drug−SA complex is transported through blood plasma; (iv) finally, it is transferred to its acceptor site or dose parts in a competitive manner. Bovine serum albumin (BSA) is a SA protein with several biochemical applications and is frequently utilized in biological studies because it contains 76% of its sequence with human serum albumin. This protein is noted for obtaining larger conformational flexibility to a wide range of ligands, and it is also inexpensive.

In this study, we explore the DNA binding properties and BSA interaction capabilities of mixed-ligand ruthenium(II) complexes of the types [Ru(bpy)$_2$(L^1-L^3)](PF$_6$) (**1**−**3**), where bpy is 2,2′-bipyridine, and salicylaldimine-type bidentate ligands (Scheme 1) such as *N*-(pyrid-2-yl)salicylaldimine [**H**(**L**^{1})], *N*-(6-methylpyrid-2-yl)salicylaldimine [**H**(**L**^{2})], and *N*-(4,6-dimethylpyrid-2-yl)salicylaldimine [**H**(**L**^{3})]. The salicylaldimine-type bidentate ligands containing coordinative N$_{imine}$ and O$_{phenolate}$ donors constitute similar RuN$_5$O chromophores in **1**−**3** with two bpy ligands and exhibit subtle variation in the dangling pyridine ring due to the absence or presence of electron-donating methyl substitution [**H**(**L**^{1}), no methyl; **H**(**L**^{2}), 6-methyl; **H**(**L**^{3}), 4,6-dimethyl]. It is believed that the (stereochemical) connection between the ligand surroundings of chemical nucleases and DNA[25,26] is essential for obtaining high DNA cleavage efficiency and cytotoxicity. Electronic effects have been demonstrated to be quite crucial in the cleavage mechanism even though steric effects play a major role. Therefore, the ability to efficiently synthesize a few structurally identical ligands with small differences in their steric and electronic configurations is necessary to optimize and completely comprehend a chemical nuclease system. As a group, salicylaldimine-type ligands are made up of a flexible and kinetically nonlabile ligand template that allows both the steric and electronic properties of the central metal ion to be modified in a synthetically simple way.[25,26] Although salicylaldimine-type ligands have a wide range of synthetic and mechanistic possibilities, electronic tuning has been nearly completely restricted to aliphatic or aromatic groups bonded to an imine nitrogen atom. Until recently, there has not been any practical synthesis of salicylaldimine-type ligands containing a dangling heterocycle, in which both sterics and electronics can be manipulated in the same ligand environment. Interestingly, the present ruthenium(II) complexes (**1**−**3**) of salicylaldimine-type ligands containing a dangling pyridine display similar structural, spectral, and electrochemical properties as well as possess more or less the same DNA binding and BSA interaction behavior, but there is distinct DNA cleavage activity and cytotoxicity because of the presence of both steric and electronic properties in the same ligand.

https://doi.org/10.1021/acs.inorgchem.1c03399
Inorg. Chem. 2022, 61, 2864−2882

EXPERIMENTAL SECTION

Materials and Methods. Ruthenium trichloride trihydrate (Arora Mathey), agarose (Genei), and ethidium bromide (EthBr; Merck) were utilized as supplied. 2,2′-Bipyridine, salicylaldehyde, 2-aminopyridine, 2-amino-6-picoline, 4,6-dimethyl-2-aminopyridine, and calf-thymus (CT) DNA (stored at −20 °C) were purchased from Sigma-Aldrich. Invitrogen Life Technologies provided the ΦX174 supercoiled phage DNA (0.25 $\mu g\ \mu L^{-1}$), which was kept at −20 °C. Bovine serum albumin (BSA) was acquired from Sigma-Aldrich and kept at 4 °C. Ultrapure Milli-Q water (18.2 mΩ) was utilized for all studies. The solvents were acquired from Biosolve (AR grade) and employed immediately in the syntheses. The precursor *cis*-$[Ru(bpy)_2Cl_2]\cdot 2H_2O$ was synthesized following the procedure in the literature.[27]

MCF7 (breast cancer), EVSA-T (breast cancer), WIDR (colon cancer), IGROV (ovarian cancer), M19 (melanoma), A498 (renal cancer), and H226 (nonsmall cell lung cancer) were among the seven human tumor cell lines employed. The WIDR, M19, A498, IGROV, and H226 cell lines are from an anticancer screening panel of the National Cancer Institute, USA.[28] MCF7 and EVSA-T are estrogen receptor (ER)+/progesterone receptor (PgR)+ and (ER)−/(PgR)− human breast cancer cell lines, respectively. A mycoplasma test was performed on all cell lines prior to the tests, and this turned out to be negative. All cell lines were grown in a continuous logarithmic culture in RPMI 1640 (Gibco, Invitrogen, Paisley, Scotland) media with 4-(2-hydroxyethyl)-1-piperazineethanesulfonic acid and phenol red. The medium was supplemented with 10% fetal calf serum (Gibco, Invitrogen, Paisley, Scotland), 100 units mL^{-1} penicillin (Sigma, St. Louis, MO), and 100 g mL^{-1} streptomycin (Sigma, St. Louis, MO). For passage and use in the study, the cells were slightly trypsinized.

Physical Measurements. Kindly consult the Supporting Information for the details of physical measurements.

Synthesis of Ligands. A solution of salicylaldehyde (3.1 g, 0.025 mol) in methanol (10 mL) was added, under constant stirring, to a solution of 2-aminopyridine (2.4 g, 0.025 mol), 2-amino-6-picoline (2.6 g, 0.025 mol), or 4,6-dimethyl-2-aminopyridine (3.1 g, 0.025 mol) in methanol (30 mL). The reaction mixture was refluxed (70 °C) for 2 h. Methanol was evaporated to dryness under reduced pressure to yield an orange oily residue. The oily material was redissolved in warm CH_2Cl_2 (20 mL) and left at room temperature for 12 h. The orange-yellow crystals were collected, washed with diethyl ether, and dried in a vacuum.

*N-(Pyrid-2-yl)salicylaldimine [**H(L^1)**]*. Yield: 4.0 g, 80%. ^{1}H NMR (DMSO-d_6, 300 MHz): group I, δ 6.986 (d, 1H, H3E), 7.456 (t, 1H, H4E), 6.975 (t, 1H, H5E), 7.765 (d, 1H, H6E), 13.041 (s, 1H, −OH); group II, δ 7.426 (d, 1H, H3F), 7.893 (t, 1H, H4F), 7.342 (t, 1H, H5F), 8.524 (d, 1H, H6F), 9.485 (s, 1H, −CH═N−) ppm. IR (neat): 3424, 3054, 2563, 1651, 1607, 1588, 1575, 1558, 1497, 1466, 1455, 1430, 1352, 1278, 1232, 1185, 1146, 1111, 1044, 1030, 1004, 994, 960, 915, 879, 845, 789, 780, 744, 733, 676, 624, 578, 563, 528, 503 cm^{-1}. ESI-MS: *m*/*z* 199 [(M + H)$^+$]. Anal. Calcd for $C_{12}H_{10}N_2O$: C, 72.71; H, 5.08; N, 14.13. Found: C, 72.36; H, 5.14; N, 14.03.

*N-(6-Methylpyrid-2-yl)salicylaldimine [**H(L^2)**]*. Yield: 4.5 g, 85%. ^{1}H NMR (DMSO-d_6, 300 MHz): group I, δ 6.971 (d, 1H, H3E), 7.420 (t, 1H, H4E), 6.939 (t, 1H, H5E), 7.785 (d, 1H, H6E), 13.109 (s, 1H, −OH); group II, δ 7.196 (d, 1H, H3F), 7.745 (t, 1H, H4F), 7.218 (d, 1H, H5F), 2.472 (s, 3H, 4-CH_3), 9.423 (s, 1H, −CH═N−) ppm. IR (neat): 3418, 3052, 2918, 1651, 1610, 1552, 1575, 1498, 1450, 1282, 1232, 1185, 1144, 992, 896, 821, 794, 757, 723, 579, 564, 548 cm^{-1}. ESI-MS: *m*/*z* 213 [(M + H)$^+$]. Anal. Calcd for $C_{13}H_{12}N_2O$: C, 73.57; H, 5.70; N, 13.20. Found: C, 73.57; H, 5.75; N, 13.39.

*N-(4,6-Dimethylpyrid-2-yl)salicylaldimine [**H(L^3)**]*. Yield: 5.0 g, 88%. ^{1}H NMR (DMSO-d_6, 300 MHz): group I, δ 6.983 (d, 1H, H3E), 7.432 (t, 1H, H4E), 6.952 (t, 1H, H5E), 7.747 (d, 1H, H6E), 13.215 (s, 1H, −OH); group II, δ 7.074 (s, 1H, H3F), 7.047 (s, 1H, H5F), 2.315 (s, 3H, 4-CH_3), 2.455 (s, 3H, 6-CH_3), 9.432 (s, 1H, −CH═N−) ppm. IR (neat): 3477, 3064, 2918, 1648, 1603, 1542, 1498, 1452, 1370, 1279, 1196, 1145, 1118, 1040, 994, 899, 846, 794, 754, 729, 616, 576, 562, 536, 520 cm^{-1}. ESI-MS: *m*/*z* 227 [(M + H)$^+$]. Anal. Calcd for $C_{14}H_{14}N_2O$: C, 74.31; H, 6.24; N, 12.38. Found: C, 74.31; H, 6.26; N, 12.57.

Synthesis of Ruthenium(II) Complexes. The complexes $[Ru(bpy)_2(L^1)]PF_6$ (**1**), $[Ru(bpy)_2(L^2)]PF_6$ (**2**), and $[Ru(bpy)_2(L^3)]PF_6$ (**3**) were prepared by using the following general procedure. A 0.260 g sample of $[Ru(bpy)_2Cl_2]\cdot 2H_2O$ was heated to reflux in ethanol (25 mL) with stirring for 1 h. The solid ligand **H(L^1)** (0.099 g, 0.5 mmol), **H(L^2)** (0.106 g, 0.5 mmol), or **H(L^3)** (0.113 g, 0.5 mmol) and a base, *N*,*N*-diisopropylethylamine (0.1 mL), were then added to the above solution. Stirring was continued, and the mixture was heated under reflux for 6 h. The color of the solution was changed from violet to red-brown. An excess of solid NH_4PF_6 was added to precipitate the product, and the red-brown crystalline solids thus formed were filtered off and washed with small amounts of cold ethanol. The solid complexes were dried *in vacuo* over P_4O_{10}. Finally, the products were recrystallized from ethanol. Yield: **1**, 0.231 g (61%); **2**, 0.246 g (64%); **3**, 0.263 g (67%).

Anal. Calcd for $C_{32}H_{25}N_6OPF_6Ru$ (**1**): C, 50.87; H, 3.34; N, 11.12. Found: C, 50.39; H, 3.06; N, 11.02. Λ_M in acetonitrile (MeCN) at 25 °C: 141 $\Omega^{-1}\ cm^2\ mol^{-1}$. ^{1}H NMR (DMSO-$d_6$, 300 MHz): δ [multiplicity, integration, assignment, coupling constant in hertz, coordination-induced shifts (c.i.s.), $\delta_{complex} - \delta_{ligand}$] 8.722 (d, 1H, H3A, 8.1, 0.339), 8.095 (t, 1H, H4A, 7.5, 0.164), 7.693 (t, 1H, H5A, 6.5, 0.257), 9.516 (d, 1H, H6A, 5.1, 0.839), 8.585 (d, 1H, H3B, 8.1, 0.202), 8.185 (t, 1H, H4B, 8.4, 0.254), 7.781 (t, 1H, H5B, 6.6, 0.345), 8.653 (d, 1H, H6B, 6.9, −0.024), 7.498 (d, 1H, H3C, 5.4, −0.885), 7.264 (t, 1H, H4C, 6.6, −0.667), 7.925 (t, 1H, H5C, 5.9, 0.489), 8.653 (d, 1H, H6C, 6.9, −0.024), 7.498 (d, 1H, H3D, 5.4, −0.885), 6.926 (t, 1H, H4D, 6.2, −1.005), 7.563 (t, 1H, H5D, 7.8, 0.127), 8.200 (d, 1H, H6D, 8.1, −0.477), 5.937 (d, 1H, H3E, 7.8, −1.049), 7.344 (t, 1H, H4E, 8.4, −0.112), 6.903 (t, 1H, H5E, 6.5, −0.072), 7.918 (d, 1H, H6E, 7.8, 0.153), 6.445 (d, 1H, H3F, 8.4, −0.981), 7.047 (t, 1H, H4F, 7.7, −0.846), 6.361 (t, 1H, H5F, 7.2, −0.981), 7.276 (d, 1H, H6F, 6.3, −1.248), 8.405 (s, 1H, −CH═N−, −1.080) ppm. Electronic spectrum in MeCN [λ_{max}/nm (ε_{max}/$dm^3\ mol^{-1}\ cm^{-1}$)]: 245 (34600), 295 (45250), 342 (9980), 371 (9560), 491 (8970), 571 sh. CV (scan rate, 50 mV s^{-1}) and DPV (2 mV s^{-1}) data in MeCN. Ligand oxidation: E_{pa}, 1.922 V; $E_{1/2}$ in DPV, 2.089 V. Ru^{III}/Ru^{II} couple: E_{pa}, 0.591 V; E_{pc}, 0.513 V; ΔE_p, 68 mV; i_{pc}/i_{pa}, 0.9; *D*, 7.4 × $10^6\ cm^2\ s^{-1}$; $E_{1/2}$ in CV, 0.547 V; $E_{1/2}$ in DPV, 0.548 V. Ru^{IV}/Ru^{III} couple: E_{pa}, 1.841 V; $E_{1/2}$ in DPV, 1.706 V. Reduction of bpy: E_{pa}, −1.651 and −2.074 V; E_{pc}, −1.740 and −1.951 V; ΔE_p, 89 and 123 mV; $E_{1/2}$ in CV, −1.700 and −2.013 V; $E_{1/2}$ in DPV, −1.719 and −2.021 V.

Anal. Calcd for $C_{33}H_{27}N_6OPF_6Ru$ (**2**): C, 51.50; H, 3.54; N, 10.92. Found: C, 51.21; H, 3.41; N, 10.86. Λ_M in MeCN at 25 °C:140 $\Omega^{-1}\ cm^2\ mol^{-1}$. ^{1}H NMR (DMSO-$d_6$, 400 MHz): δ (multiplicity, integration, assignment, coupling constant in hertz, c.i.s., $\delta_{complex} - \delta_{ligand}$) 8.717 (d, 1H, H3A, 8.0, 0.334), 8.095 (t, 1H, H4A, 8.0, 0.164), 7.687 (t, 1H, H5A, 5.2, 0.251), 9.514 (d, 1H, H6A, 4.8, 0.837), 8.602 (d, 1H, H3B, 8.0, 0.219), 8.178 (t, 1H, H4B, 7.8, 0.247), 7.771 (t, 1H, H5B, 6.6, 0.335), 8.648 (d, 1H, H6B, 6.4, −0.029), 7.506 (d, 1H, H3C, 5.2, −0.877), 7.256 (t, 1H, H4C, 5.2, −0.675), 7.929 (t, 1H, H5C, 8.0, 0.493), 8.648 (d, 1H, H6C, 6.4, −0.029), 7.465 (d, 1H, H3D, 5.2, −0.918), 7.036 (t, 1H, H4D, 7.6, −0.895), 7.552 (t, 1H, H5D, 7.8, 0.116), 8.222 (d, 1H, H6D, 8.0, −0.455), 6.401 (d, 1H, H3E, 7.2, −0.570), 6.955 (t, 1H, H4E, 7.6, −0.465), 6.343 (t, 1H, H5E, 6.4, −0.596), 7.265 (d, 1H, H6E, 6.0, −0.520), 5.930 (d, 1H, H3F, 8.0, −1.266), 7.274 (t, 1H, H4F, 6.6, −0.478), 6.731 (d, 1H, H5F, 7.6, −0.487), 2.079 (s, 3H, 6-CH_3, −0.393), 8.364 (s, 1H, −CH═N−, −1.058) ppm. Electronic spectrum in MeCN [λ_{max}/nm (ε_{max}/$dm^3\ mol^{-1}\ cm^{-1}$)]: 245 (34410), 295 (44650), 342 (10220), 371 (9190), 491 (8970), 571 sh. CV (scan rate, 50 mV s^{-1}) and DPV (2 mV s^{-1}) data in MeCN. Ligand oxidation: E_{pa}, 1.943 V; $E_{1/2}$ in DPV, 1.889 V. Ru^{III}/Ru^{II} couple: E_{pa}, 0.612 V; E_{pc}, 0.544 V; ΔE_p, 68 mV; i_{pc}/i_{pa}, 0.8; *D*, 7.4 × $10^6\ cm^2\ s^{-1}$; $E_{1/2}$ in CV, 0.578 V; $E_{1/2}$ in DPV, 0.568 V. Ru^{IV}/Ru^{III} couple: E_{pa}, 1.833 V; $E_{1/2}$ in DPV, 1.698 V. Reduction of bpy: E_{pa}, −1.741 and −2.072 V; E_{pc}, −1.649 and −1.953

https://doi.org/10.1021/acs.inorgchem.1c03399
Inorg. Chem. 2022, 61, 2864−2882

Table 1. Selected Crystal Data and Structure Refinement Parameters for 1−3

	$[Ru(bpy)_2(L^1)](PF_6)$ (1)	$[Ru(bpy)_2(L^2)](PF_6)$ (2)	$[Ru(bpy)_2(L^3)](PF_6)$ (3)
formula	$C_{32}H_{25}F_6N_6OPRu$	$C_{33}H_{27}F_6N_6OPRu$	$C_{34}H_{29}F_6N_6OPRu$
fw (g mol^{-1})	755.62	769.65	783.67
temperature (K)	293(2)	293(2)	293(2)
wavelength (Å)	0.71069	0.71069	0.71069
cryst syst	orthorhombic	monoclinic	monoclinic
space group	*Pbca*	*P*21/*n*	*P*21/*n*
a (Å)	16.5791(8)	10.4489(7)	10.9642(9)
b (Å)	18.4378(9)	20.8610(13)	20.9054(16)
c (Å)	20.3836(10)	15.1307(9)	15.1969(12)
α (deg)	90	90	90
β (deg)	90(10)	102(10)	105.891(2)
γ (deg)	90	90	90
V $(Å)^3$, *Z*	6230.9(5), 8	3218.7(4), 4	3350.2(5), 4
D_{calc} (g cm^{-3})	1.611	1.588	1.554
μ (mm^{-1})	0.628	0.610	0.587
F(000)	3040	1552	1584
cryst size (mm^3)	0.27 × 0.24 × 0.20	0.23 × 0.18 × 0.16	0.20 × 0.16 × 0.15
θ (deg)	1.93−29.60	1.69−28.22	1.70−29.00
index ranges	$-22 \le h \le 22, -24 \le k \le 25, -27 \le l \le 26$	$-13 \le h \le 13, -27 \le k \le 27, -19 \le l \le 19$	$-14 \le h \le 14, -27 \le k \le 28, -20 \le l \le 19$
reflns collected	75188	34523	43292
indep reflns	8264	7398	8707
reflns obsd $[I > 2\sigma(I)]$	4928	5031	4573
R_{int}	0.0458	0.0311	0.0468
GOF	1.008	1.018	1.003
R_1, $wR_2[I > 2\sigma(I)]$	0.0487, 0.0890	0.0835, 0.2550	0.0510, 0.1354
R_1, wR_2 (all data)	0.0887, 0.1612	0.1089, 0.2765	0.1039, 0.1518

V; ΔE_p, 92 and 119 mV; $E_{1/2}$ in CV, −1.695 and −2.013 V; $E_{1/2}$ in DPV, −1.719 and −2.032 V.

Anal. Calcd for $C_{34}H_{29}N_6OPF_6Ru$ (**3**): C, 52.11; H, 3.73; N, 10.72. Found: C, 51.85; H, 3.54; N, 10.70. Λ_M in MeCN at 25 °C: 141 Ω^{-1} cm^2 mol^{-1}. ^1H NMR (DMSO-d_6, 400 MHz): *δ* (multiplicity, integration, assignment, coupling constant in hertz, c.i.s., $\delta_{complex} - \delta_{ligand}$) 8.714 (d, 1H, H3A, 8.0, 0.331), 8.091 (t, 1H, H4A, 8.0, 0.160), 7.689 (t, 1H, H5A, 6.6, 0.253), 9.516 (d, 1H, H6A, 5.6, 0.839), 8.632 (d, 1H, H3B, 8.0, 0.249), 8.191 (t, 1H, H4B, 7.8, 0.260), 7.776 (t, 1H, H5B, 6.6, 0.340), 8.653 (d, 1H, H6B, 7.6, −0.024), 7.534 (d, 1H, H3C, 5.2, −0.849), 7.266 (t, 1H, H4C, 6.6, −0.665), 7.933 (t, 1H, H5C, 7.8, 0.497), 8.653 (d, 1H, H6C, 7.6, −0.024), 7.444 (d, 1H, H3D, 5.2, −0.939), 6.954 (t, 1H, H4D, 6.6, −0.977), 7.559 (t, 1H, H5D, 7.6, 0.123), 8.246 (d, 1H, H6D, 8.0, −0.431), 6.423 (d, 1H, H3E, 8.4, −0.560), 7.025 (t, 1H, H4E, 7.8, −0.407), 6.347 (t, 1H, H5E, 7.6, −0.605), 7.273 (d, 1H, H6E, 7.2, −0.474), 5.532 (s, 1H, H3F, −1.542), 6.550 (s, 1H, H5F, −0.497), 1.914 (s, 3H, 4-CH_3, −0.401), 2.038 (s, 3H, 6-CH_3, −0.417), 8.363 (s, 1H, −CH═N−, −1.069) ppm. Electronic spectrum in MeCN [λ_{max}/nm (ε_{max}/dm^3 mol^{-1} cm^{-1})]: 245 (37550), 295 (46840), 342 (10590), 371 (10320), 491 (9310), 571 sh. CV (scan rate, 50 mV s^{-1}) and DPV (2 mV s^{-1}) data in MeCN. Ligand oxidation: E_{pa}, 2.080 V; $E_{1/2}$ in DPV, 1.940 V. Ru^{III}/Ru^{II} couple: E_{pa}, 0.569 V; E_{pc}, 0.502 V; ΔE_p, 67 mV; i_{pc}/i_{pa}, 0.9; *D*, 7.2 × 10^6 cm^2 s^{-1}; $E_{1/2}$ in CV, 0.536 V; $E_{1/2}$ in DPV, 0.545 V. Ru^{IV}/Ru^{III} couple: E_{pa}, 1.803 V; $E_{1/2}$ in DPV, 1.668 V. Reduction of bpy: E_{pa}, −1.734 and −2.071 V; E_{pc}, −1.642 and −1.952 V; ΔE_p, 92 and 119 mV; $E_{1/2}$ in CV, −1.688 and −2.012 V; $E_{1/2}$ in DPV, −1.719 and −2.032 V.

X-ray Crystallographic Procedures. Upon slow evaporation of an ethanolic solution of the respective complex, single crystals of **1**−**3** were formed. A crystal of **1**, **2**, or **3** was mounted on a glass fiber using epoxy cement. A Bruker SMART APEX CCD diffractometer with a fine-focus sealed-tube Mo K*α* X-ray source was used to collect X-ray diffraction data. The intensity data for all of the crystals were recorded using the *ω*-scan technique. Data acquisition was done using *SMART* software, and data were extracted using *SAINT*. Empirical absorption corrections were made on the intensity data.[29] The space group for **1** was assigned as *Pbca*, while **2** and **3** were assigned as $P2_1/n$ using systematic absences and *E* statistics of the data set. These space groups were later confirmed by successful structure solution and refinement. The details of data collection and structure analysis are given in Table 1. A direct method was used to solve the structures of **1**, **2**, or **3** using the *SIR97*[30] program and refined with the *SHELXL 97* program[31] using the full-matrix least-squares method on F^2. Anisotropic refinement was applied to all non-hydrogen atoms. We found no disorder in PF_6^- for **2**. Six fluorine atoms in the PF_6^- anion for **1** and **3** were disordered. Site occupancies of the disordered fluorine atoms were refined, and their sum was limited to one. The hydrogen atoms in the complex were fixed in place and refined with the help of a riding model. The goodness-of-fit (GOF) values of 1.008(1), 1.018(2), and 1.003(3) were achieved during final refinement of the structures of **1**−**3**. Selected bond lengths and angles are furnished in Table 2.

DNA and Protein Binding Experiments. The ratio of UV absorbances at 260 and 280 nm, A_{260}/A_{280}, of DNA solutions in a 5 mM Tris HCl/50 mM NaCl buffer was 1.9,[32] suggesting that the DNA was adequately free of protein.

The stock solution of protein (1.0 × 10^{-4} mol L^{-1}) was prepared by dissolving solid BSA in a 0.05 M phosphate buffer at pH 7.4, stored at 0−4 °C in the dark for about 1 week, and then diluted to 1.0 × 10^{-6} mol L^{-1} using a phosphate buffer (pH 7.4, 0.05 M) upon use. The concentration of BSA was determined from optical density measurements, using a value of the molar absorptivity ε_{280} of 44720 M^{-1} cm^{-1}.[33] The detailed procedure for the spectroscopic experiments of DNA and protein binding as well as the electrochemical experiments for DNA binding is described in the Supporting Information.

DNA Cleavage Experiments. In the pH-dependent DNA cleavage test, a 2.5 mM ruthenium(II) complex in 0.1 M phosphate buffer, pH 6.0−8.0 in 0.5 step increments, was incubated for 4 h with 0.05 μg μL^{-1} ΦX174 RF supercoiled phage DNA. The DNA damage was evaluated by comparing the electrophoretic movement of the species in a 1% agarose gel, prepared in a 1 × TBE buffer, to those of the control incubations: control 2 examined the activity of the

https://doi.org/10.1021/acs.inorgchem.1c03399
Inorg. Chem. 2022, 61, 2864−2882

Table 2. Selected Bond Lengths (Å) and Bond Angles (deg) for 1−3

	$[Ru(bpy)_2(L^1)](PF_6)$ (1)		
N1−Ru1	2.067(3)	N3−Ru1	2.066(3)
N4−Ru1	2.059(3)	N5−Ru1	2.035(3)
N6−Ru1	2.043(3)	O1−Ru1	2.074(2)
O1−Ru1−N1	89.53(11)	O1−Ru1−N3	87.94(11)
O1−Ru1−N4	88.72(11)	O1−Ru1−N5	171.98(11)
O1−Ru1−N6	94.49(11)	N1−Ru1−N3	96.84(11)
N1−Ru1−N4	175.45(12)	N1−Ru1−N5	94.59(12)
N1−Ru1−N6	86.62(11)	N3−Ru1−N4	78.90(12)
N3−Ru1−N5	98.38(12)	N3−Ru1−N6	175.80(11)
N4−Ru1−N5	87.66(12)	N4−Ru1−N6	97.71(12)
N5−Ru1−N6	78.92(12)		
	$[Ru(bpy)_2(L^2)](PF_6)$ (2)		
N1−Ru1	2.066(5)	N3−Ru1	2.059(5)
N4−Ru1	2.032(5)	N5−Ru1	2.018(5)
N6−Ru1	2.041(5)	O1−Ru1	2.083(4)
O1−Ru1−N1	88.98(19)	O1−Ru1−N3	88.9(2)
O1−Ru1−N4	89.30(19)	O1−Ru1−N5	172.7(2)
O1−Ru1−N6	94.6(2)	N1−Ru1−N3	95.4(2)
N1−Ru1−N4	174.2(2)	N1−Ru1−N5	93.9(2)
N1−Ru1−N6	89.1(2)	N3−Ru1−N4	79.0(2)
N3−Ru1−N5	97.5(2)	N3−Ru1−N6	174.36(19)
N4−Ru1−N5	88.5(2)	N4−Ru1−N6	96.6(2)
N5−Ru1−N6	78.8(2)		
	$[Ru(bpy)_2(L^3)](PF_6)$ (3)		
N1−Ru1	2.065(3)	N3−Ru1	2.057(3)
N4−Ru1	2.049(3)	N5−Ru1	2.028(3)
N6−Ru1	2.038(3)	O1−Ru1	2.074(2)
O1−Ru1−N1	89.38(12)	O1−Ru1−N3	90.11(12)
O1−Ru1−N4	87.14(11)	O1−Ru1−N5	171.26(13)
O1−Ru1−N6	93.45(13)	N1−Ru1−N3	95.48(13)
N1−Ru1−N4	173.29(13)	N1−Ru1−N5	94.89(13)
N1−Ru1−N6	86.86(13)	N3−Ru1−N4	78.80(14)
N3−Ru1−N5	97.05(12)	N3−Ru1−N6	175.76(13)
N4−Ru1−N5	89.34(12)	N4−Ru1−N6	99.07(14)
N5−Ru1−N6	79.21(14)		

complex under assay settings that are known to cause DNA retardation (as above but with no phosphate buffer), and control 1 was DNA in conditions identical with those of control 2 but without the complex. From each test, 20 μL was added with 4 μL of dye (0.025 mg of bromophenol blue, 1 mL of glycerol, and 1 mL of Milli-Q water) and pipetted into wells on the horizontal gel. A potential difference of 40 mV was applied for 3 h to the gel, and the bands were observed using EthBr staining. A similar experiment was carried out in the absence of a complex to evaluate the effect of pH alone on DNA.

T4 Ligase-Religation Studies. An enzymatic study was carried out using T4 DNA ligase to find out whether the cleaved products were consistent with hydrolysis of the phosphodiester linkages in DNA. For the religation tests, the solution was incubated for 18 h at 16 °C prior to gel electrophoresis. The nicked circular (NC) DNA obtained from the hydrolytic cleavage reaction was recovered from agarose gel by a phenol extraction method and purified by ethanol precipitation. This was followed by the addition of a 10× ligation buffer and T4 DNA ligase (4 units) to the purified NC DNA.

Sulforhodamine B (SRB) Test. The complexes were dissolved to a concentration of 5 mg mL^{-1} in DMSO (Sigma, St. Louis, MO) and subsequently diluted to a final concentration of 250000 ng mL^{-1} in a full medium. The cytotoxicity was estimated by a microculture SRB test.[34] The Supporting Information contains a detailed procedure for the SRB test.

RESULTS AND DISCUSSION

Syntheses of Ligands and Ruthenium(II) Complexes. Condensation reactions of 2-aminopyridine, 2-amino-6-picoline, or 4,6-dimethyl-2-aminopyridine with salicylaldehyde in refluxing methanol for 2 h lead to new heterofunctionalized phenol−imine bidentate ligands containing imine nitrogen (N_{imine}) and phenolate oxygen ($O_{phenolate}$) donors and dangling pyridine [$\mathbf{H(L^1)}$], 6-methylpyridine [$\mathbf{H(L^2)}$], or 4,6-dimethylpyridine [$\mathbf{H(L^3)}$] in high yields. The three ligands primarily differ concerning the nature of the substituent(s) present in the pyridine ring connected to the N_{imine} atom. The anionic forms of the ligands (L^{1-3}) are expected to bind to the metal ion in a bidentate N,O manner, forming a six-membered chelate ring. The ligands are soluble in a range of organic solvents and are stable to hydrolysis and aerial oxidation. The strong broad band observed at 3418−3477 cm^{-1} in the spectra is assigned to the ν(OH) vibration. The Schiff bases display their C═N band within the wavenumber range 1648−1651 cm^{-1}. The phenolic C−O of $\mathbf{H(L^1)}$−$\mathbf{H(L^3)}$ is observed at 1278−1282 cm^{-1}. A weak band observed at 992−994 cm^{-1} is ascribed to the aldehydic ν(CH) (−CH═N−) vibration.

The reaction of $\mathbf{H(L^1)}$, $\mathbf{H(L^2)}$, or $\mathbf{H(L^3)}$ in the presence of a base (*N*,*N*-diisopropylethylamine) with 1 equiv of $[Ru(bpy)_2Cl_2]\cdot 2H_2O$ in ethanol at reflux gave a red-brown solution, from which a pure crystalline red-brown solid precipitated upon the addition of NH_4PF_6; the addition of a base was necessary to deprotonate the hydroxyl group and render it a better coordination site. The microanalytical data were as expected in accordance with the formation of $[Ru(bpy)_2(L^1/L^2/L^3)]PF_6$, in which L^1, L^2, or L^3 acts as a monoanionic phenolate−imine bidentate donor, and they were confirmed by X-ray structure analysis. Conductivity experiments indicate that they behave as 1:1 electrolytes in a MeCN solution. The maximum molecular peaks are observed from electrospray ionization mass spectrometry (ESI-MS) spectra at *m*/*z* 610.7 (**1**), 624.7 (**2**), and 638.7 (**3**), which match well with the corresponding calculated masses (**1**, *m*/*z* 611.1; **2**, *m*/*z* 625.1; **3**, *m*/*z* 639.1) of the monocations. As expected, the free Schiff-base phenolic OH stretching[35] (~3400 cm^{-1}) is not observed in the IR spectrum of the complex. The C═N stretching[36] is observed as a strong peak around 1600 cm^{-1} with a bathochromic shift between 37 and 49 cm^{-1}, which is typical for coordinated imines of this type.[37] The diamagnetic complexes **1**−**3** correspond to the bivalent state of ruthenium (low-spin d^6, $S = 0$).

Description of the Crystal Structures. The ORTEP views of $[Ru(bpy)_2(L^1)]^+$ (**1**), $[Ru(bpy)_2(L^2)]^+$ (**2**), and $[Ru(bpy)_2(L^3)]^+$ (**3**) are illustrated in Figure 1A−C. The crystal structures of the complexes contain a racemic mixture of Λ/Δ enantiomeric pairs. In the structures of **1**−**3**, the ruthenium(II) ion is coordinated by the two bidentate bpy ligands and a monoanionic phenolate−imine bidentate Schiff-base ligand, which forms a RuN_5O chromophore in a distorted octahedral geometry, as can be seen from the angles subtended at the metal. The average cis and trans angles are 88.65(12)° (**1**), 88.15(5)° (**2**), or 88.94(13)° (**3**) and 174.41(11)° (**1**), 173.75(8)° (**2**), or 173.44(13)° (**3**), respectively. Distortion of the coordination sphere is primarily caused by the two acute (~79°) bite angles of the two juxtaposed bpy chelate rings. The halves of the bpy ligands are nearly coplanar with dihedral angles of 5.5 and 4.2° (**1**), 5.4 and 1.7° (**2**), and 1.4 and 5.3° (**3**) about the 2,2′ bond. The bite angles of the phenolate−

https://doi.org/10.1021/acs.inorgchem.1c03399
Inorg. Chem. 2022, 61, 2864−2882

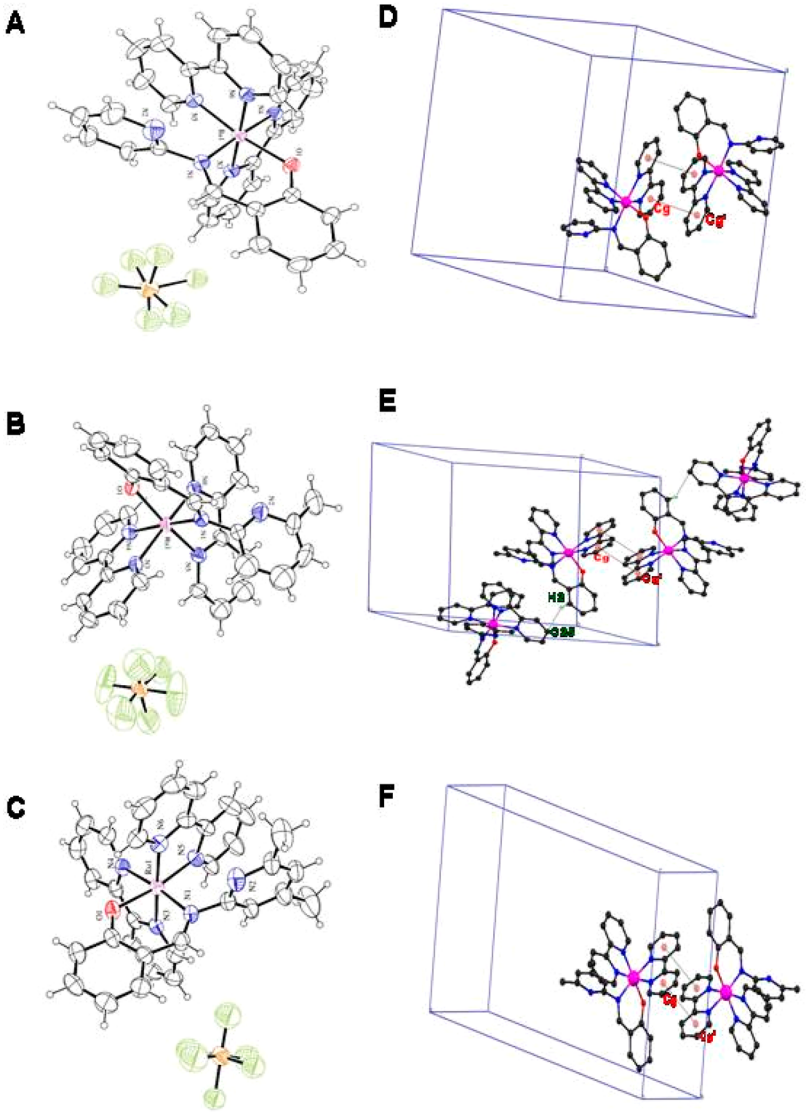

Figure 1. ORTEP views of **1** (A), **2** (B), and **3** (C) with atom numbering of the complex cation and thermal ellipsoids at 40% probability. Packing diagrams D−F showing the $\pi-\pi$ interaction (dotted lines) in $[Ru(bpy)_2(L^1)]^+$ (**1**), the $\pi-\pi$ and C−H···π interactions (dotted lines) in $[Ru(bpy)_2(L^2)]^+$ (**2**), and the $\pi-\pi$ interaction (dotted lines) in $[Ru(bpy)_2(L^3)]^+$ (**3**), respectively.

imine chelate, 89.53(11)° (**1**), 88.98(19)° (**2**), and 89.38(12)° (**3**), are very close to the ideal value.

The $Ru-N_{bpy}$ bond lengths within each complex are slightly different and lie in the ranges 2.035(3)−2.066(3) Å (**1**), 2.018(5)−2.059(5) Å (**2**), and 2.028(3)−2.057(3) Å (**3**), which bracket the Ru−N distance in $[Ru(bpy)_3]^{2+}$ [2.056(6) Å].[38] The shortest $Ru-N_{bpy}$ distance is to the nitrogen atom trans to the σ-donating phenolate, which is consistent with improved $Ru(d\pi) \rightarrow bpy(\pi^*)$ back-bonding due to the increased electron density at the metal center. The Ru−N1 [**1**, 2.067(3) Å; **2**, 2.066(5) Å; **3**, 2.065(3) Å] bond length (N_{imine} atom of L^1-L^3) is almost similar to that of Ru−N3 of the cis-coordinated bpy moiety, indicating that the N_{imine} atom is more strongly bound similar to the nitrogen atom of bpy but longer than the $Ru-N_{imine}$ distance found in $[Ru(bpy)_2(HNCHC_6H_4O)]^+$, 2.039(4) Å.[39] The ruthenium phenolate moiety is essentially planar. $Ru-O_{phenolate}$ is observed to be 2.074(2) Å (**1**), 2.083(4) Å (**2**), or 2.074(2) Å (**3**), which is also longer than 2.060(3) Å observed in $[Ru(bpy)_2(HNCHC_6H_4O)]^+$.[39] The longer bond distances in **1**−**3** are probably due to the steric effect arising from the six-membered chelate ring or may be a steric hindrance of the dangling pyridine of L^1-L^3. The Ru−N2 distance is 3.86 Å (**1**), 3.63 Å (**2**), or 3.81 Å (**3**), revealing that there is no interaction with the seventh coordinating atom.

The $Ru-N_{imine}$ bond length is shorter than the $Ru-O_{phenolate}$ despite the fact that $O_{phenolate}$ is a better σ-donor. The bond distance of N1−C7 is 1.305(5) (**1**) or 1.278(9) (**2**) or 1.301(5) Å (**3**), which is normal for a C = N double bond.[40] However, closer examination of salicylaldimine of L^1 (**1**) bond distances show that the C2−C3 [1.372(6) Å] and C4−C5 [1.373(6) Å] are shorter than C1−C2 [1.416(5) Å], C3−C4 [1.377(7) Å], C5−C6 [1.414(6) Å] and C6−C1 [1.427(5) Å]. Also, C6−C7 [1.426(5) Å] is shorter than that observed for the free ligand (1.448 Å).[38] Similarly, the imine bond C7−N1 [1.305(5) Å] is longer than in the free ligand (1.285 Å) and the phenolate bond C1−O1 [1.299(6) Å] is shorter than in the free ligand (1.348 Å). These trends in $Ru-O_{phenolate}$ and $Ru-N_{imine}$ distances and distances within the salicylaldimine

https://doi.org/10.1021/acs.inorgchem.1c03399
Inorg. Chem. 2022, 61, 2864−2882

Scheme 2. Ligand Orientation and Proton Numbering Pattern for 1−3

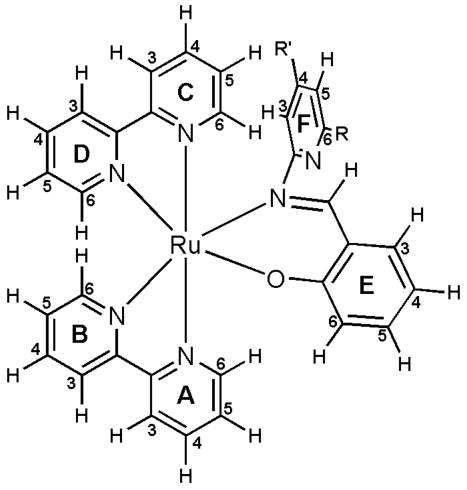

R = R' = H **1**
R = -CH_3; R' = H **2**
R = R' = -CH_3 **3**

unit support a description of significant delocalization of the negative charge between the N_{imine} and $O_{phenolate}$ atoms.

The X-ray crystal structure[41] of the free ligand **H(L^1)** reveals that both molecules are planar and that the dangling pyridine ring has the same orientation with respect to the rest of the molecule (salicylaldimine moiety). However, in the complexes, the increased interplanar angles observed at 78.3° (**1**), 73.6° (**2**), and 84.3° (**3**) indicate that the dangling pyridine ring has a perpendicular orientation with respect to the salicylaldimine unit. It is worth mentioning that the lattice structures[42] of **1**−**3** are further stabilized by $\pi-\pi$-stacking interactions because of intermolecular interactions between 2,2′-bipyridine ligands (Figure 1D−F) with Cg···Cg′ distances of 3.840 Å (**1**), 3.946 Å (**2**), and 3.853 Å (**3**) (Cg and Cg′ are the N3/C13−C17 and N4/C18−C22 ring centroids) and interplanar angles of 6.53° (**1**), 5.19° (**2**), and 6.09° (**3**). These $\pi-\pi$ aromatic interactions in **2** are further reinforced by C−H···π interactions (Figure 1E) via atoms C2−H2 of the phenolate ring and C25 of one of the bpy rings with a distance of 3.328 Å.

^{1}H NMR Spectra. The chemical shifts of the free and coordinated ligands (Scheme 2) are summarized in the Experimental Section, along with coordination-induced shifts (c.i.s. = $\delta_{complex} - \delta_{ligand}$) and coupling constants. The J values were compatible with the spectral assignments, which were based on the COSY spectra of the complexes.

The ^{1}H NMR spectra of free ligands (HL^1−HL^3) could be mainly classified into two groups (I and II). Group I has five resonances, and the chemical shifts are typical for salicylaldimine derivatives.[43] The peaks correspond to the protons of the phenol moieties [**H(L^1)**−**H(L^3)**, H3−H6, and −OH]. This suggests that the Schiff bases exist in the enolimine form in a DMSO solution. The two **H(L^3)**, three **H(L^2)**, or four **H(L^1)** aromatic resonances and the one **H(L^2)** or two **H(L^3)** aliphatic resonances found for group II are assigned to the protons of the corresponding pyridine rings connected to the N_{imine} atom. The most significant signal in the spectra is a singlet (δ = 9.4−9.5 ppm), which is assigned to the azomethine (−CH═N−) proton. As expected, the resonances for the protons H3−H6 of the phenol moiety are unaffected by the pyridine group attached to the N_{imine} atom. Interestingly, the nature of the substituent present in the pyridine ring connected to the N_{imine} atom severely affects the chemical shift of the protons of the −CH═N− and −OH functions. Notably, the −CH═N− and −OH protons in the analogous tetradentate ligand appear at δ = 8.7 and 11.4 ppm, respectively.[39] A downfield shift is observed for both protons of all of the ligands relative to the tetradentate ligand, which is ascribed to the effect of the ring current associated with the conjugated system. It seems that this invariability in the present investigation is caused by a rather strong hydrogen-bonding interaction between the hydrogen atom of the phenolic −OH and the nitrogen atom of the imine group. Such hydrogen bonding is not present in the aforementioned salicylaldimine-type tetradentate ligand. The X-ray crystal structure[41,43] of the free ligand **H(L^1)** reveals that the molecule is planar and that the dangling pyridine ring has the same orientation for the rest of the molecule (salicylaldimine moiety). For instance, the pyridine nitrogen atom is always oriented cis to the hydrogen atom of the imine group, which indicates a strong intramolecular hydrogen-bonding interaction. The orders of the protons in increasing field strength are **H(L^1)** > **H(L^2)** ≈ **H(L^3)** (−CH═N−) and **H(L^3)** > **H(L^2)** > **H(L^1)** (−OH). These observations reveal (i) an increase in the van der Waals interaction between the azomethine proton and the nitrogen lone pair of 2-pyridine, **H(L^1)**, and (ii) a stronger intramolecular hydrogen bonding between the hydrogen atom of the phenolic −OH and the nitrogen atom of the imine group in **H(L^3)** relative to **H(L^1)** and **H(L^2)**.

The ^{1}H NMR spectra of the complexes display 24 (**1**), 23 (**2**), or 21 (**3**) nonequivalent aromatic signals (Figure 2) due to the presence of an unsymmetric salicylaldimine moiety in **1**−**3**, which makes all six aromatic rings nonequivalent. The absence of a phenolic −OH proton of the free ligands **H(L^1)**−**H(L^3)** in the spectra of the complexes suggests coordination through $O_{phenolate}$ of **H(L^1)**−**H(L^3)**. Therefore, the equatorial plane contains one pyridine ring from each of the two bpy ligands (rings B and D: H3−H6), the oxygen atom of the phenolate group (ring E: H3−H6), and the azomethine nitrogen atom of **H(L^1)**−**H(L^3)**. The axial positions are occupied by the other pyridine rings of the bpy ligands (rings A and C: H3−H6), while the uncoordinated pyridine ring (ring F: **1**, H3−H6; **2**, H3−H5 and 6-CH_3; **3**, H3, H5, and 4- and 6-CH_3) of **H(L^1)**−**H(L^3)** is dangling. When coordinated to ruthenium(II), the planar bpy rings are expected to form a five-membered chelate ring with an envelope conformation and the unsymmetric salicylaldimine moiety of **H(L^1)**−**H(L^3)** forms a six-membered chelate ring with a twist boat conformation, as in the X-ray crystal structures of **1**−**3**.

https://doi.org/10.1021/acs.inorgchem.1c03399
Inorg. Chem. 2022, 61, 2864−2882

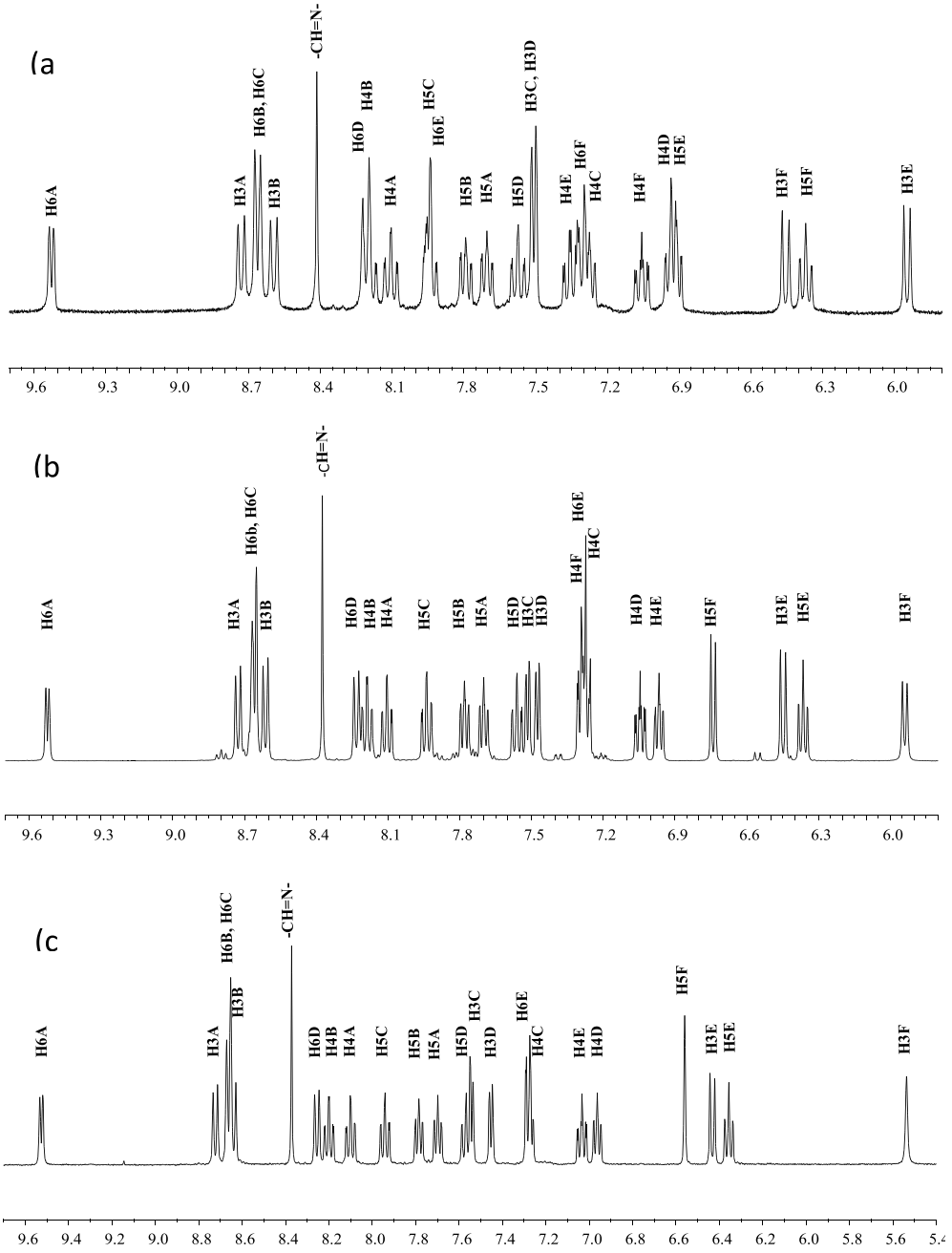

Figure 2. ^{1}H NMR spectra of (a) **1**, (b) **2**, and (c) **3** in $(CD_3)_2SO$.

Thus, the observable singlet of the azomethine (−CH═N−) proton of the salicylaldimine moiety is shielded at 8.405 ppm (**1**), 8.364 ppm (**2**), or 8.363 ppm (**3**) compared to free ligands (9.422−9.485 ppm), resulting in negative c.i.s. values. The azomethine proton is likely close to ruthenium(II) and hence experiences electron density around it because of the twist boat conformation imposed by the six-membered chelate ring. The most upfield signals appearing for ring D protons (H3−H6), which are trans to $O_{phenolate}$, are significantly different from the other resonances because the ring experiences a trans effect of the σ-donor phenolate function. The order of the pyridine ring protons in increasing field strength appears to be 6 > 3 > 4 > 5 for rings A and B, but for rings C and D, it is 6 > 5 > 3 > 4. The protons of the phenolate function follow the order 6 > 4 > 5 > 3 for **1**, but for **2** and **3**, it is 6 > 5 > 3 > 4. The 6-CH_3 (2.079 ppm) and the 4-CH_3 (1.914 ppm) and 6-CH_3 (2.038 ppm) upfield signals of **2** and **3**, respectively, appear as singlets. Because coordination forces the pyridine rings of bpy to be coplanar, the dangling pyridine ring in $\mathbf{H(L^2)}$/$\mathbf{H(L^3)}$ is obliged to rotate away from bpy to minimize the steric interactions with bpy, and hence the 6-CH_3 (**2**) and 4- and 6-CH_3 (**3**) protons of a dangling pyridine ring are exposed to the shielding magnetic anisotropy due to the ring currents of the pyridine ring of bpy.

The large positive c.i.s. value for H6**A** (**1**-**3**) proton arise from an σ-effect based on electron donation to Ru(II) *via* the nitrogen lone pairs. A negative c.i.s. value observed for the H6**D** (**1**-**3**) proton, adjacent to the coordinating nitrogen, would result from interligand through-space ring-current anisotropy effects and there is a lesser influence on H6**B** and

https://doi.org/10.1021/acs.inorgchem.1c03399
Inorg. Chem. 2022, 61, 2864−2882

H6**C** (**1**-**3**) protons. Similarly, the complexes show a negative c.i.s. values for H3**C**, H4**C**, H3**D**, H4**D**, H3**F**, and H5**F** (**1**-**3**), H4**F** (**1**,**2**), and H6**F** (**1**) protons due to the magnetic anisotropy induced by proximate ring current. In coordination with Ru(II), the H3**E** (**1**) and H3**E**-H6**E** (**2**,**3**) protons signal is shifted upfield due to Ru(II) to ligand π-back-donation, which has a lesser influence on the H4**E** and H5**E** (**1**) protons. The positive c.i.s. values observed for H3**A** and H3**B** (**1**-**3**) protons are obviously due to van der Waals interaction. Further, the positive c.i.s. values for H4**A**, H5**A**, H4**B**, H5**B**, H5**C** and H5**D** (**1**-**3**) and H6**E** (**1**) protons suggest that the ligand-to-metal σ-donation is more important (as this will decrease the electron density at these sites leading to positive c.i.s. values) than metal-to-ligand π-back-donation in the ground state of these complexes.

Electronic Spectral Properties. The absorption spectra of **2** and **3** are virtually identical with those obtained for compound **1**. These spectra are similar[39] to that of $[Ru(bpy)_2(HN{=}CH\text{-}C_6H_4O)]^+$ except for the presence of an intense band at 342 nm, and the bands are slightly blue-shifted with higher absorptivity. In the visible region, the complexes exhibit two transitions at 491 and 371 nm. The lower-energy transition (491 nm) is associated with a shoulder at lower energy (571 nm). First, the two visible bands (491 and 371 nm) have been assigned based on the reported spectra of $[Ru(bpy)_2]^{2+}$ complexes having other kinds of chelating ligands.[44,45] There are two different kinds of bipyridine π^*-acceptor orbitals involved in the $d\pi(Ru^{II}) \rightarrow \pi^*(bpy)$ metal-to-ligand charge-transfer (MLCT) transitions, one symmetric (χ) and one antisymmetric (ψ) concerning the C_2 axis of the ligand,[44b,46] and the transition from metal-filled dπ orbitals to these two π^* orbitals results in the above-mentioned bands. The lower-energy band at 491 nm is due to $d\pi(Ru^{II}) \rightarrow \pi^*(\psi)$ and the higher-energy band at 371 nm to $d\pi(Ru^{II}) \rightarrow \pi^*(\chi)$, approximately 6580 cm^{-1} higher in energy than the former, as expected. Second, an absorption maximum at 342 nm is observed with nearly the same intensity ($\varepsilon \approx 10000$ dm^3 mol^{-1} cm^{-1}) as that of the other two visible bands. This can be interpreted as follows: (i) This may be due to a metal-centered d−d transition similar to $[Ru(bpy)_3]^{2+}$ (340 nm); this increased intensity is consistent with the lower symmetry and is also likely to have a contribution from intensity borrowing from other charge-transfer bands.[47] (ii) This is expected because transitions in the MLCT region are expected to appear due to the $d\pi(Ru^{II}) \rightarrow \pi^*$(imine) transition.[48] Finally, the two intense bands observed at 245 and 295 nm are characteristic of ligand-centered $\pi-\pi^*$ transitions and very similar to the analogous absorptions of $[Ru(bpy)_3]^{2+}$. The lowest-energy MLCT transition of $[Ru(bpy)_3]^{2+}$ appears at 450 nm;[48] therefore, replacement of one bpy ligand by an asymmetric ligand **H**($\mathbf{L^1}$), **H**($\mathbf{L^2}$), or **H**($\mathbf{L^3}$) results in a red shift of the same transition. The negative charge erected on the metal by the strongly σ-donating phenolate moiety would be predicted to destabilize the metal dπ orbital, reducing the $d\pi \rightarrow \pi^*$ MLCT band energy relative to $[Ru(bpy)_3]^{2+}$.

Redox Behavior. Complexes **1**−**3** display a redox wave ($E_{1/2}$: **1**, 0.55 V; **2**, 0.58 V; **3**, 0.54 V versus Ag/AgCl) that corresponds to the Ru^{II}/Ru^{III} couple based on the magnitude of the diffusion coefficients [D, (7.2−7.4) × 10^6 cm^2 s^{-1}] calculated from cyclic voltammetry (CV) at different scan rates (30−500 mV). The i_{pa} versus $\nu^{1/2}$ plots, which pass through the origin, are linear, indicating that the redox processes at the electrode are diffusion-controlled. The peak potential separations ΔE_p (67−68 mV) are larger than the Nernstian value of 59 mV for a one-electron transfer; they are typical for complexes of this kind, owing to uncompensated solution resistance.[49] The substitution of one π-acidic bpy ligand from the $[Ru(bpy)_3]^{2+}$ core by one σ-donating **H**($\mathbf{L'}$) in **1**−**3** results in a decrease of the Ru^{II}/Ru^{III} potential. This is due to a reduction of the overall charge of the complex cation from 2+ in $[Ru(bpy)_3]^{2+}$ to 1+ in **1**−**3**, which provides electrostatic stabilization of the oxidized Ru^{III}-L′ species. Other RuN_5O chromophoric systems, $[Ru^{II}(bpy)_2(L')]^+$, exhibit the Ru^{II}/Ru^{III} couple at 0.52−0.77 V.[39] The similarity of the Ru^{II}/Ru^{III} potential of **1**−**3** with that of the *N*-salicylaldimine system further supports the close ligand-field strengths of these classes of complexes. Complexes **1**−**3** (E_{pa}, **1**, 1.84; **2**, 1.83; **3**, 1.80) also exhibit a second irreversible oxidation wave. The one-electron nature is confirmed by differential pulse voltammetry (DPV). It could be due to either the Ru^{II}/Ru^{III} couple or oxidation of the ligand. However, the free ligands **H**($\mathbf{L^1}$)−**H**($\mathbf{L^3}$) exhibit an irreversible oxidation wave [E_{pa}: **H**($\mathbf{L^1}$), 1.31 V; **H**($\mathbf{L^2}$), 1.21 V; **H**($\mathbf{L^3}$), 1.22 V], and their E_{pa} values are substantially lower (500−600 mV) than the ruthenium(II) complexes. In addition, the potential difference between the two successive oxidation couples is ∼1.2 V, which agrees well with the average potential difference between the redox couples of the ruthenium center ($Ru^{II/III}$ − $Ru^{III/IV}$ ∼ 1.0−1.5 V) observed in other mononuclear complexes.[50] Therefore, the second irreversible oxidation wave corresponds to the Ru^{III}/Ru^{IV} couple. Further, two successive quasi-reversible ligand-based reductions are also observed for all of the complexes, the one-electron nature of which is established by the magnitude of the peak currents, which may involve the addition of electrons in the electrochemically accessible lowest unoccupied molecular orbital (LUMO)[51] of the diimine (−N=C−C=N−) fragment of bpy.

Resonance Raman Spectra. The electrochemical and electronic spectral data presented above strongly suggest that the LUMO of **1**−**3** is localized at the bpy ligand. To further substantiate these assignments, we carried out resonance Raman experiments at 532 nm, which is preresonant with 491 nm and postresonant with 571 nm absorption bands of these complexes. At this excitation wavelength, the modes associated with both the bpy and Schiff-base ligands, **H**($\mathbf{L^1}$)−**H**($\mathbf{L^3}$), become enhanced. Inspection of the resonance Raman spectra (Figure S1) indicates no change in the pattern with an increase in the number of methyl groups at the dangling pyridine moiety, which might be expected because of their similar structures. The high-energy features in the spectra at 1602 and 1554 cm^{-1} [both ν(C=C)], 1480 cm^{-1} (the most intense one), 1312 cm^{-1} [both ν(C=N)], and 1270 cm^{-1} [ν(C=C) inter-ring] and peaks with a shoulder at 1164/1154 cm^{-1} [δ(CCH) in plane] and 1020/1036 cm^{-1} (ring breathing) are ascribable to the internal modes of the coordinated bpy ligands,[52] and this is confirmed by the spectral shifts (20−30 cm^{-1}) induced in these bands upon deuteration of bpy. In the low-frequency end of the spectra, there are bands at 664 cm^{-1} [δ(CCC) inter-ring, isotope sensitive] and 374 cm^{-1}; the former has been tentatively associated with a ligand-deformation mode of bpy and the latter with a symmetric $Ru-N_{bpy}$ stretching mode.[53] The band at 374 cm^{-1} shows only a weak resonance enhancement because the MLCT transition exerts little influence on the $Ru-N_{bpy}$ bond. On the basis of these results, we conclude that the broad absorption with a maximum near 491 nm is assigned as a $Ru^{II}(d\pi) \rightarrow bpy(\pi^*)$

https://doi.org/10.1021/acs.inorgchem.1c03399
Inorg. Chem. 2022, 61, 2864−2882

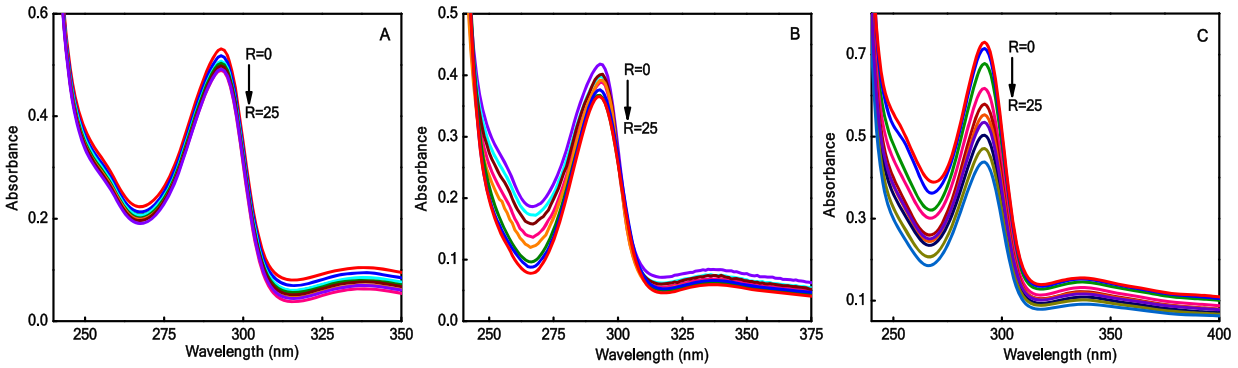

Figure 3. Absorption spectra of **1** (A), **2** (B), and **3** (C) (3.0×10^{-5} M) in 2% DMF/5 mM Tris-HCl/50 mM NaCl buffer at pH 7.1 in the absence ($R = 0$) and presence ($R = 25$) of increasing amounts of CT DNA.

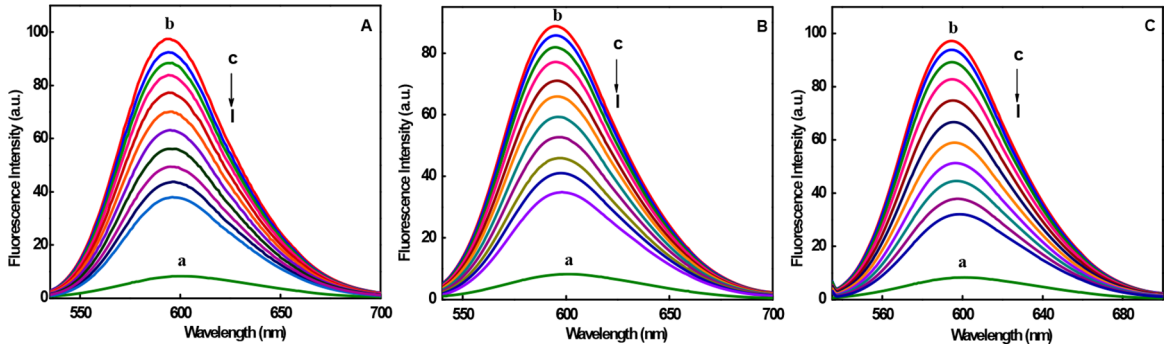

Figure 4. Fluorescence quenching curves of EthBr bound to DNA in a 2% DMF/5 mM Tris-HCl/50 mM NaCl buffer at pH 7.1: (a) EthBr (1.25 μM); (b) EthBr + DNA (125 μM); (c–m) EthBr + DNA + **1** (A), **2** (B), and **3** (C) (0–10 μM).

MLCT transition. This was anticipated because the Schiff-base ligands, $\mathbf{H(L^1)}$–$\mathbf{H(L^3)}$, containing phenolate and imine functionalities possess no empty low-lying energy levels. These results indicate that the first reduction potential is bpy-based and the first oxidation potential is metal-based, which is in agreement with the electrochemical measurements.

Further, the high-energy shoulders observed at 1484 and 1316 cm^{-1} are assigned to ν(C═N) stretching vibrations due to the imine functionality of $\mathbf{H(L^1)}$–$\mathbf{H(L^3)}$, and a weak low-frequency feature at 428 cm^{-1} might best be considered as the Ru–N_{imine} stretching mode. The weak feature at 1526 cm^{-1} and shoulders at approximately 1474 and 1606 cm^{-1}, obscured by the bpy features at 1602 and 1554 cm^{-1}, are attributed to the phenolate functionality because they are insensitive to deuteration of the bpy moieties.[54] Furthermore, bands observed at 1422, 1388, and 1264 cm^{-1} and features at 622, 598, 524, and 478 cm^{-1} (**1**), 618, 572, 528, and 476 cm^{-1} (**2**), and 622, 570, 530, and 470 cm^{-1} (**3**) are associated with the phenolate functionality of $\mathbf{H(L^1)}$–$\mathbf{H(L^3)}$. On the basis of a comparison with other oxygen-bound complexes,[55] the band in the range 570–598 cm^{-1} is assigned to Ru–O stretching vibrations. These features are distinctly enhanced by the transition at 571 nm. These observations, in conjunction with the simultaneous presence of bpy-centered modes, suggest that the longest-wavelength absorbance in these complexes is associated with an $\mathbf{H(L)}(\pi) \rightarrow$ bpy(π^*) interligand charge-transfer (ILCT) transition due to the loss of electron density on the oxygen because the electron is transferred from the oxygen lone pair of phenolate in $\mathbf{H(L^1)}$–$\mathbf{H(L^3)}$ to π^* of the bpy units. The interpretation of these resonance Raman effects would require separate normal-mode and molecular orbital calculations, which have not yet been attempted.

DNA Binding Studies. Upon the incremental addition of CT DNA to **1**–**3** (Table S1), the ligand-centered $\pi \rightarrow \pi^*$ absorption band (293 nm) of **1** shows a slight decrease in the molar absorptivity (hypochromism: **1**, ~10%) with no red shift, while **2** exhibits a slight increase and **3** displays a significant increase in the molar absorptivity (hyperchromism: **2**, ~14%; **3**, ~42%) (Figure 3) at $R = 25$ (R = [DNA]/[Ru]), suggesting a strong interaction between the ruthenium(II) complexes and DNA. The spectral change might be interpreted as due to groove binding of the adducts[56] because **1**–**3** containing fused polyaromatic systems having coplanar atoms (organic ligand) facilitates the formation of van der Waals contacts or hydrogen bonds during interaction with the DNA grooves. The intrinsic binding constant, K_b, values of **1** (6.97×10^4 M^{-1}), **2** (7.22×10^4 M^{-1}), and **3** (7.55×10^4 M^{-1}) are almost the same (Figure S2), which is expected because of their very similar molecular structures.[57] These values are in agreement with those of a well-established groove binding rather than classical intercalation.[58]

Upon the addition of **1**–**3** (0–10 μM) to CT DNA pretreated with EthBr ([EthBr]/[DNA] = 0.01) in a 2% DMF/5 mM Tris-HCl/50 mM NaCl buffer at pH 7.1 (Figure 4), the emission intensity at 595 nm of DNA-bound EthBr decreases (% quenching: **1**, ~71%; **2**, ~68%; **3**, ~76%), revealing that the ruthenium(II) complexes competitively bound to CT DNA with EthBr. The observation of EthBr fluorescence quenching due to the release of some EthBr molecules from the EthBr/DNA system is supportive of the interaction of **1**–**3** with CT DNA through groove binding.[59] According to the Stern–Volmer equation, the relative binding propensity (K_{SV}: **1**, 5.21×10^4 M^{-1}; **2**, 4.58×10^4 M^{-1}; **3**, 7.51×10^4 M^{-1}) of the complex to CT DNA was determined from

https://doi.org/10.1021/acs.inorgchem.1c03399
Inorg. Chem. 2022, 61, 2864–2882

Table 3. Electrochemical Data[a] for the Ruthenium(II) Complexes in the Presence and Absence of CT DNA

				$E_{1/2}$ (V)					
complex	R	E_{pc} (V)	E_{pa} (V)	CV	DPV[b]	ΔE_p (mV)	i_{pc}/i_{pa}	D ($\times 10^6$ cm^2 s^{-1})	K_{2+}/K_{3+}
1	0	0.373	0.431	0.402	0.376	59	0.73	5.8	0.969
	5	0.371	0.431	0.401	0.376	60	1.08	5.9	
2	0	0.358	0.432	0.395	0.369	73	1.02	4.9	0.962
	5	0.358	0.436	0.397	0.370	77	1.13	5.1	
3	0	0.360	0.423	0.391	0.368	63	0.82	4.9	0.925
	5	0.360	0.428	0.394	0.369	67	1.35	4.7	

[a]Measured versus standard calomel electrode. Scan rate: 50 mV s^{-1}. Supporting electrolyte: 5 mM Tris-HCl/50 mM NaCl. Complex concentration: 2.5 × 10^{-4} M. [b]DPV. Scan rate: 2 mV s^{-1}. Pulse height: 50 mV.

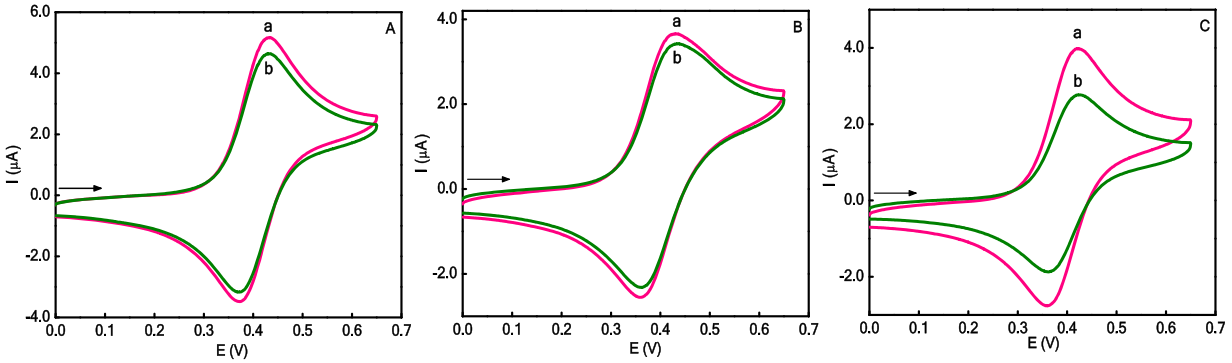

Figure 5. Cyclic voltammograms of **1** (A), **2** (B), and **3** (C) (0.5 mM) in the absence (a) and presence (b) of CT DNA (R = 5) at 25.0 ± 0.2 °C and a 50 mV s^{-1} scan rate in a 2% DMF/5 mM Tris-HCl/50 mM NaCl buffer at pH 7.1.

the slope of a straight line (Figure S3) obtained from the plot of the fluorescence intensity versus the complex concentration.[60] The fluorescence quenching curve of EthBr-bound CT DNA by **1**−**3** showed that quenching of the EthBr/DNA system by **1**−**3** is in good agreement with the linear Stern−Volmer equation, which also indicates that the complexes bind to DNA. According to the equation K_{EthBr}[EthBr] = K_{app}[complex], where K_{EthBr} is 4.94 × 10^5 M^{-1},[61] the concentration of EthBr is 1.25 × 10^{-6} M and the concentration of the complex is that used to obtain a 50% reduction of fluorescence intensity of EthBr. The K_{app} values are calculated to be 8.82 × 10^4 M^{-1} (**1**), 8.23 × 10^4 M^{-1} (**2**), and 9.50 × 10^4 M^{-1} (**3**), and the apparent binding constant decreases in the order **2** < **1** < **3**, which is less than the binding constant of the classical intercalators and metallointercalators (10^7 M^{-1}). The K_{app} value is consistent with the K_b value obtained by the UV−vis absorption spectral study, suggesting that the interaction of **1**−**3** with DNA is a groove binding mode.[62]

The circular dichroism (CD) spectrum of CT DNA was monitored (Table S2) in the presence of **1**−**3** at a 1/R (=[Ru complex]/[DNA]) value of 3; the positive band showed little increase in the molar ellipticity (**1**, ∼14%; **2**, ∼10%; **3**, ∼18%), and the negative band displayed a small decrease in the molar ellipticity (**1**, ∼18%; **2**, ∼12%; **3**, ∼12%) with no red or blue shift of the band maxima (Figure S4, curve b). These observations are supportive of the groove binding mode of interaction of **1**−**3**, which is consistent with the results obtained from the UV−vis absorption and fluorescence spectral studies.

The CV and DPV responses were obtained for **1**−**3** on a glassy carbon electrode in a 2% DMF/5 mM Tris-HCl/50 mM NaCl buffer at pH 7.1 in the presence and absence of DNA, and the well-behaved CV and DPV responses are used to monitor the interaction of the complexes with DNA (Table 3). The redox potentials of the Ru^{II}/Ru^{III} couple ($E^{0\prime}$ or voltammetric $E_{1/2}$) for **1**−**3** (**1**, 0.402 V; **2**, 0.395 V; **3**, 0.391 V) are consistent with the general trends in $E_{1/2}$ values in a MeCN solution (cf. above). Upon the addition of CT DNA to **1**−**3** (R = 5), a drop in the peak currents of both anodic and cathodic waves in the CV (Figures 5 and S5) and DPV responses (Figure S6) is observed. The intensity of the peak current (**1**, ∼14%; **2**, ∼10%; **3**, ∼21%) decreases with the addition of DNA, and the decrease is higher for **3** than for others, which is consistent with the above spectral studies. This indicates the slower mass transfer of **1**−**3** bound to DNA fragments,[63] which leads to a decrease in the concentration of the unbound redox-active species in solution. It can be observed that **1**−**3** exhibit more or less the same electrochemical behavior in both the DNA-free and -bound complexes, such as the formal potentials ($E_{1/2}$) of the Ru^{II}/Ru^{III} couple (DNA-free/DNA-bound: **1**, 0.402/0.401 V; **2**, 0.395/0.397 V; **3**, 0.391/0.394 V), peak potential separation ΔE_p (DNA-free/DNA-bound: **1**, 59/60 mV; **2**, 73/77 mV; **3**, 63/67 mV), and the diffusion coefficient D (DNA-free/DNA-bound: **1**, 5.8/5.9 × 10^6 cm^2 s^{-1}; **2**, 4.9/5.1 × 10^6 cm^2 s^{-1}; **3**, 4.9/4.7 × 10^6 cm^2 s^{-1}), revealing that **1**−**3** interact with CT DNA in a groove binding fashion. The values of K_{2+}/K_{3+} were determined using the Nernst equation and found to be in the range of 0.925−0.969 for ruthenium(II) complexes, whose potential shift is 1−3 mV. Interestingly, a K_{2+}/K_{3+} value of near-unity for **1**−**3** shows that they are involved in DNA interaction, favoring both of the oxidation states equally.[64]

BSA Interaction. The BSA solution has a strong fluorescence emission peak at 340 nm when excited at 280 nm. Therefore, the emission spectra of BSA (1 × 10^{-6} M) in the presence of increasing concentrations of **1**−**3** [(1−4.5) × 10^{-6} M] were recorded at 300 and 310 K (Table 4). The fluorescence intensity of BSA decreased regularly (Figure 6),

https://doi.org/10.1021/acs.inorgchem.1c03399
Inorg. Chem. 2022, 61, 2864−2882

Table 4. Quenching, Association, Binding, and Thermodynamic Parameters of the Interaction of 1−3 with BSA at Different Temperatures

parameters	300 K	R	310 K	R
	$[Ru(bpy)_2(L^1)]^+$ (**1**)			
K_{SV} (10^4 M^{-1}) ± SD	5.264 ± 0.002	0.9992	5.751 ± 0.002	0.9989
k_q (10^{12} M^{-1} s^{-1})	5.264		5.751	
K_a (10^4 M^{-1}) ± SD	5.053 ± 0.005	0.9992	5.521 ± 0.004	0.9995
K_b (10^4 M^{-1}) ± SD	5.063 ± 0.098	0.9969	5.575 ± 0.100	0.9968
n ± SD	0.987 ± 0.017		0.994 ± 0.017	
$\Delta H°$ (kJ mol^{-1})	77.951			
$\Delta S°$ (J mol^{-1} K^{-1})	90.303		91.032	
$\Delta G°$ (kJ mol^{-1})	−27.013		−28.142	
	$[Ru(bpy)_2(L^2)]^+$ (**2**)			
K_{SV} (10^4 M^{-1}) ± SD	4.018 ± 0.004	0.9988	4.739 ± 0.004	0.9998
k_q (10^{12} M^{-1} s^{-1})	4.018		4.739	
K_a (10^4 M^{-1}) ± SD	4.619 ± 0.003	0.9996	4.899 ± 0.002	0.9998
K_b (10^4 M^{-1}) ± SD	4.203 ± 0.120	0.9952	4.431 ± 0.112	0.9961
n ± SD	0.982 ± 0.02		0.992 ± 0.01	
$\Delta H°$ (kJ mol^{-1})	77.742			
$\Delta S°$ (J mol^{-1} K^{-1})	89.556		90.037	
$\Delta G°$ (kJ mol^{-1})	−26.789		−27.833	
	$[Ru(bpy)_2(L^3)]^+$ (**3**)			
K_{SV} (10^4 M^{-1}) ± SD	6.347 ± 0.005	0.9988	6.952 ± 0.001	0.9995
k_q (10^{12} M^{-1} s^{-1})	6.347		6.952	
K_a (10^4 M^{-1}) ± SD	5.809 ± 0.004	0.9997	6.247 ± 0.010	0.9984
K_b (10^4 M^{-1}) ± SD	6.553 ± 0.077	0.9982	6.873 ± 0.082	0.9979
n ± SD	0.996 ± 0.014		0.996 ± 0.014	
$\Delta H°$ (kJ mol^{-1})	77.830			
$\Delta S°$ (J mol^{-1} K^{-1})	91.462		92.058	
$\Delta G°$ (kJ mol^{-1})	−27.361		−28.460	

up to 35% (**1**), 25% (**2**), and 49% (**3**) at 300 K and 38% (**1**), 30% (**2**), and 50% (**3**) at 310 K, accompanied by a blue shift of 7−9 nm. All of the Stern−Volmer plots[65] (Figure S7) represent a good linear relationship. As is known, linear Stern−Volmer plots represent a single quenching mechanism, either static (the ground-state complex formation between a quencher and a fluorophore) or dynamic (a collisional process).[66] The value of the Stern−Volmer quenching constant (K_{SV}) is obtained from the slope of the plot F_0/F versus [Q] at different temperatures. The value of the quenching rate constant (k_q) is obtained from the equation $K_{SV} = k_q\tau_0$. The result shows that K_{SV} increases with rising temperature (Table 4), indicating that the fluorescence quenching of BSA by ruthenium(II) complexes is likely to occur via a dynamic quenching mechanism. The maximum value of k_q of various quenchers with biological macromolecules is 10^{10} M^{-1} s^{-1}.[67] In the present study, the k_q values of the quenching processes (~10^{12} M^{-1} s^{-1}) are greater than 10^{10} M^{-1} s^{-1}. These results suggest that the quenching is not initiated by a dynamic mechanism but originates from the formation of a ground-state complex, resulting from the static quenching mechanism.[68]

Alternatively, the UV−vis absorption spectra of BSA in the absence and presence of **1−3** were recorded (Figure 7) to explore the structural changes of BSA and to investigate formation of the BSA−complex system (a static quenching process). The UV−vis spectrum of BSA has two main absorption peaks. The strong absorption peak around 210 nm reflects absorption of the backbone of BSA, and the weak absorption peak around 280 nm is due to the aromatic acid residues.[69] With the addition of **1−3**, the intensity of the peak at 210 nm decreased with an ~6 nm (**1**), ~8 nm (**2**), or ~13 nm (**3**) red shift and the intensity of the peak at 280 nm increased slightly. The results indicate that the interaction between **1−3** and BSA leads to the loosening and unfolding of the BSA backbone and an increase in the hydrophobicity of the microenvironment of BSA. It is well-known that dynamic quenching does not change the absorption spectrum, but formation of the nonfluorescence ground-state complex can change it,[66] and thus the interaction between **1−3** and BSA was mainly a static quenching process.

Therefore, the quenching data were analyzed according to the modified Stern−Volmer equation.[70] The modified Stern−Volmer plots (Figure S8) reveal a good linear relationship, and the corresponding effective quenching constant (K_a) increases with rising temperature (Table 4), following the dependence of K_{SV} on the temperature as mentioned above. The results show that the binding constants between the ruthenium(II) complexes and BSA are moderate. It is noted that the binding constant of 10^4−10^6 M^{-1} is acceptable for drug-carrier complexes.[71] Thus, the binding constants of **1−3** show that BSA can be considered to be a good carrier for transfer of these ruthenium(II) complexes *in vivo*.

For the static quenching interaction, if it is assumed that there are similar and independent binding sites in the biomolecule, the number of complex bound per protein (n) and binding constant (K_b) can be calculated using a double-logarithmic equation.[72] As shown in Figure S9, the double-logarithmic plot is a straight line. The values of K_b and n can be obtained from the intercept and slope of the plot, respectively, at two different temperatures (Table 4). The results reveal that the values of the binding constants with BSA increase with rising temperature, which is due to an enhancement in the stability of the BSA−complex system and shows that the binding process is an endothermic reaction.[73] All of the binding constants are medium and indicate that the interaction between BSA and the ruthenium(II) complexes is moderate. The values of n at the experimental temperatures are approximately equal to 1, which indicates that there is just a single binding site[74] in BSA for **1−3**. In addition, BSA has two tryptophan residues that have intrinsic fluorescence. Trp-212 is located within a hydrophobic binding pocket, and Trp-134 is located on the surface of the molecule. A linear Stern−Volmer plot is generally indicative of a single class of fluorophore, all equally accessible to the quencher. These molecules do not rapidly penetrate the hydrophobic interior of proteins, and only those tryptophan residues on the surface of the protein are quenched. Accordingly, three similar complexes most likely bind to Trp-134 in BSA.[75]

The calculated values of $\Delta G°$, $\Delta H°$, and $\Delta S°$ at two different temperatures are given in Table 4. The value of $\Delta G°$ is negative, so the binding process is spontaneous. The values of

https://doi.org/10.1021/acs.inorgchem.1c03399
Inorg. Chem. 2022, 61, 2864−2882

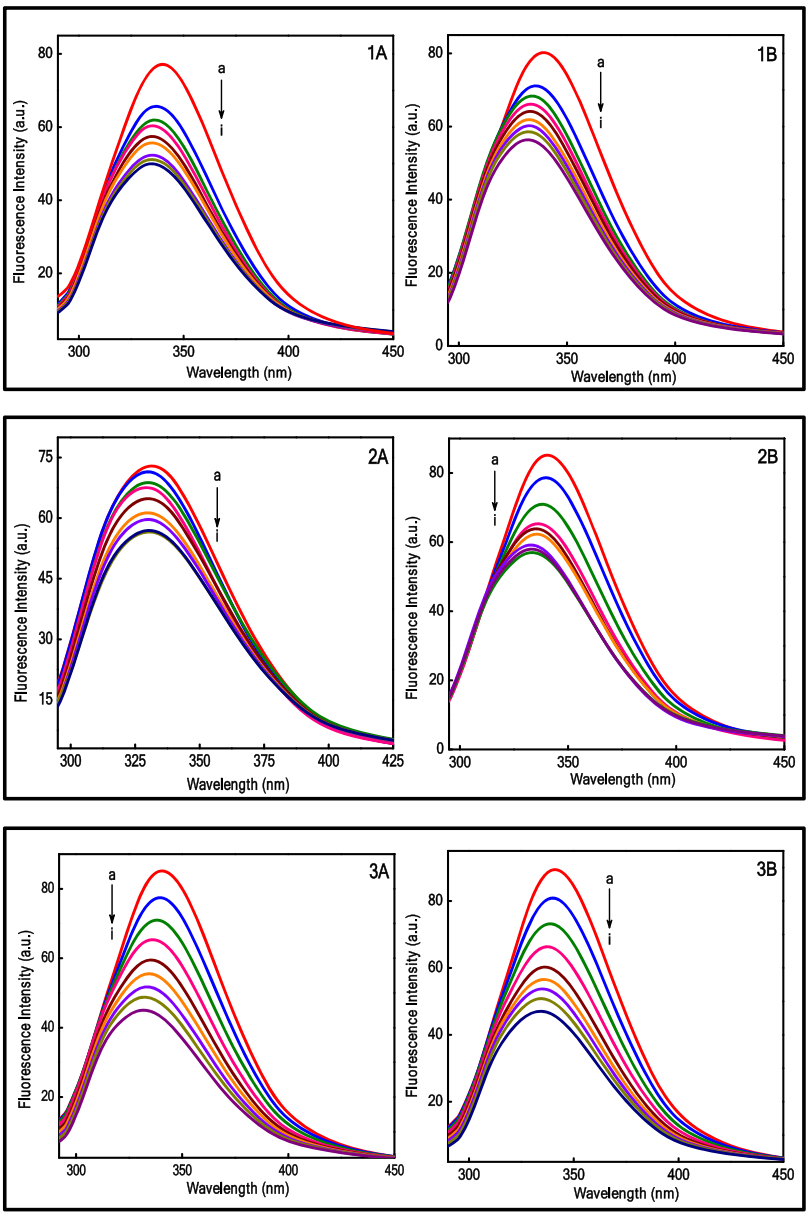

Figure 6. Changes in the fluorescence spectra of BSA through titration with complexes **1**−**3** at 300 K (left, A) and 310 K (right, B). The concentration of BSA is 1×10^{-6} mol L^{-1}, and the concentration of **1**−**3** was varied from (a) 0.0 to (i) 4.5×10^{-6} mol L^{-1}, with pH 7.4 and λ_{ex} = 280 nm.

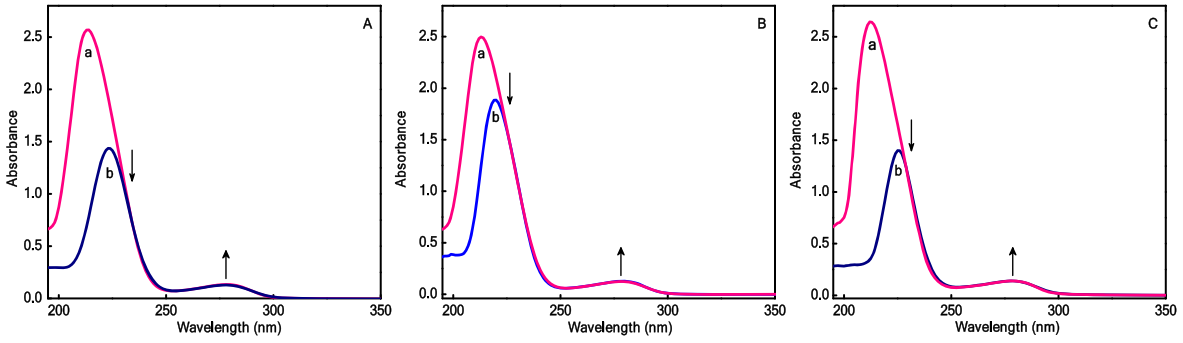

Figure 7. UV−vis absorption spectra of BSA in the absence and presence of **1** (A), **2** (B), and **3** (C): (a) Absorption spectrum of BSA. (b) Absorption spectrum of BSA in the presence of **1**−**3** at the same concentration, [BSA] = [Cu complex] = 3.5×10^{-6} mol L^{-1}. The absorbance of **1**−**3** is negligible in the spectral region shown.

https://doi.org/10.1021/acs.inorgchem.1c03399
Inorg. Chem. 2022, 61, 2864−2882

Figure 8. Agarose gel showing cleavage of 20 μM ΦX174 RF DNA incubated with 2.5 mM **1** (A), **2** (B), and **3** (C) in a 0.1 M phosphate buffer at 37 °C for 4 h. Lane 1: DNA control. Lanes 2–6: DNA + **1** (A), **2** (B), or **3** (C). (pH 8.0, 7.5, 7.0, 6.5, and 6.0, respectively.) Forms I and II are the SC and NC forms of DNA, respectively.

Scheme 3. Protonation of the Dangling Pyridine Moiety of Schiff-Base Ligands (1–3), Postulated as Being Responsible for pH-Dependent Damage to DNA

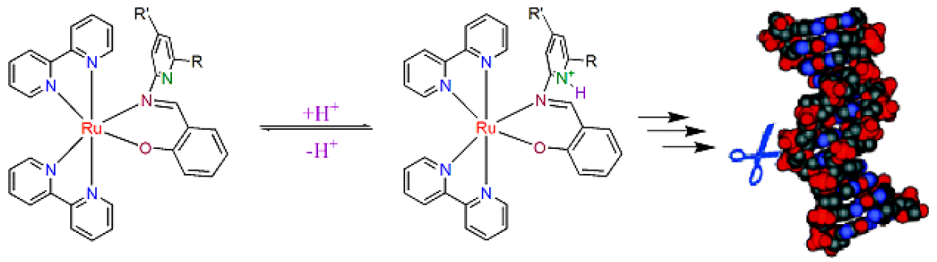

$\Delta H°$ and $\Delta S°$ are positive. The positive value of $\Delta H°$ shows that the binding process is mainly an endothermic reaction. The greater negative values of $T\Delta S°$ compared to $\Delta H°$ reveal that the formation of a complex between **1–3** and BSA is mainly an entropy-driven reaction and $T\Delta S°$ governs the spontaneity of the reaction. The positive $\Delta H°$ and $\Delta S°$ values indicate that the hydrophobic interaction is the main force in the binding of **1–3** to BSA.

pH-Dependent DNA Cleavage. To assess the DNA cleavage ability of the complexes, supercoiled plasmid ΦX174 RF DNA (20 μM) was incubated for 4 h with **1–3** (2.5 mM) in the absence of an activator in a 0.1 M phosphate buffer, pH 6.0–8.0 in 0.5 step increments. When plasmid DNA is nicked in its supercoiled form (form I), an open circular relaxed form (form II) is generated, and with further cleavage, a linear form (form III) is produced. When electrophoresis is performed on the reaction mixture, the compact form I migrates relatively faster, while the nicked form II migrates more slowly and the linearized form (form III) migrates between forms I and II. The ΦX174 RF DNA substrate used in agarose gel electrophoresis is 95% supercoiled (SC), 5% nicked circular (NC), and 0% linear circular, and their positions can be distinguished on the gel (Figure 8, lane 1). The results show that when DNA is incubated with **1–3** at pH 7.5 or 8.0 (Figure 8, lanes 2 and 3), the DNA migrates similarly to the DNA substrate (SC, 95%; NC, 5%). However, at pH 7.0 (Figure 8, lane 4), the SC form of DNA incubated with **1–3** is slightly retarded (SC, 90%; NC, 10%) compared to the substrate DNA (SC, 95%; NC, 5%). Interestingly, when the pH is reduced to 6.5 or 6.0 (Figure 8, lanes 5 and 6), all of the complexes show a sudden increase in retardation because of the stronger cleavage properties [pH 6.5/6.0: **1**, SC (15/8), NC (85/90), LC (0/2); **2**, SC (10/5), NC (90/90), LC (0/5); **3**, SC (5/3), NC (90/87), LC (5/10)]. This indicates that **1–3** convert form I into form II and then into form III at pH 6.0, while at pH 6.5, **3** cleaves form I into form II and then into form III but **1** and **2** convert form I into form II alone. It was proposed that for the dangling pyridine moiety in **1–3**, which contains one nitrogen atom with a pK_a value of 6.84 (**1**, 2-aminopyridine), 7.60 (**2**, 2-amino-6-picoline), or 9.50 (**3**, 2-amino-4,6-dimethylpyridine), the nitrogen atom with a high pK_a value could capture H^+ strongly and enhance the interaction with negatively charged DNA. It was found that at a pH >7 almost no damage to the DNA is observed, whereas below pH 7, DNA damage is prevalent. Because healthy cells grow at pH >7, typically pH 7.2, and (hypoxic) cancer cells have characteristically lower pH

https://doi.org/10.1021/acs.inorgchem.1c03399
Inorg. Chem. 2022, 61, 2864–2882

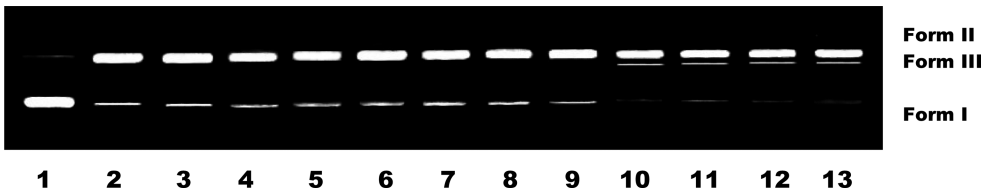

Figure 9. Agarose gel showing cleavage of 20 μM ΦX174 RF DNA incubated with 2.5 mM **1**−**3** in a 0.1 M phosphate buffer at 37 °C for 24 h (pH 6.5). Lane 1: DNA control. Lane 2: DNA + **1**. Lane 3: DNA + **1** + NaN_3 (500 μM). Lane 4: DNA + **1** + KI (500 μM). Lane 5: DNA + **1** + DMSO (20 μM). Lane 6: DNA + **2**. Lane 7: DNA + **2** + NaN_3 (500 μM). Lane 8: DNA + **2** + KI (500 μM). Lane 9: DNA + **2** + DMSO (20 μM). Lane 10: DNA + **3**. Lane 11: DNA + **3** + NaN_3 (500 μM). Lane 12: DNA + **3** + KI (500 μM). Lane 13: DNA + **3** + DMSO (20 μM).

values, typically pH 6.8, we propose that **1**−**3** might selectively target cancer cells. At the same time, we propose that the dangling pyridine moiety in **1**−**3** could be protonated at lower pH and in this form cause damage to DNA, as illustrated in Scheme 3. The ability of **1**−**3** to exhibit pH-dependent cleavage of DNA follows the order **3** > **2** > **1**. Upon replacement of the dangling pyridyl group in **1** by the 2-methylpyridyl group as in **2** and the 4,6-dimethylpyridyl group as in **3**, there is an enormous increase in the electron density on the dangling pyridyl nitrogen atom because of the presence of electron-donating methyl group(s) in **2** and **3**. This reveals the importance of the electronic effect of a substituted methyl group(s) in enriching the electron density on the dangling pyridyl nitrogen atom of **2** and **3**, thereby rendering the abstraction of H^+ more facile. On the other hand, the ability of hydrophobic interaction of the complex depends on the incorporation of a number of methyl groups in the dangling pyridyl group. As a consequence, the increase in hydrophobic interaction from **1** to **3** at a pH <6.8 can promote stronger binding to DNA and raise the cleavage activity.

For the ruthenium(II) complexes **1**−**3**, which show efficient pH-dependent DNA cleavage, mechanistic studies were performed at pH 6.5. DNA cleavage generally proceeds via two major pathways: one is hydrolytic cleavage, and the other is oxidative cleavage. The oxidative processes generally form reactive singlet oxygen or hydroxyl radical species involving a photoactive or a redox-active metal center, causing damage to the sugar and/or base and resulting in the formation of fragmented species that cannot be religated. Hydrolytic cleavage in the absence of any external additives does not suffer from such drawbacks because the cleaved products can be religated enzymatically. To investigate the role of radicals in DNA damage by **1**−**3**, cleavage reactions were carried out under aerobic conditions in the absence of an external reagent by incubating **1**−**3** with DNA for 4 h in the presence of a variety of radical scavengers like DMSO (hydroxyl radical), NaN_3 (singlet oxygen), and KI (superoxide). The results show that DNA cleavage by **1**−**3** is not inhibited by any of the classical radical scavengers (Figure 9). To ascertain the mechanism of the DNA cleavage reaction by **1**−**3**, form II (NC) obtained from the cleavage of SC DNA has been isolated, treated with a T4 ligase enzyme, and subjected to gel electrophoresis.[76] We have observed ∼73% (**1**), ∼78% (**2**), or ∼84% (**3**) conversion of form II to its original form I, indicating that a hydrolytic mechanism dominates over other mechanisms (Figure 10).

Cytotoxicity of Ruthenium(II) Complexes. The free ligand $\mathbf{H(L^1)}$−$\mathbf{H(L^3)}$ and complexes **1**−**3** have been screened against cell lines of different cancer origins, viz., renal cancer (A498), breast cancer (EVSA-T and MCF-7), nonsmall cell lung cancer (H226), ovarian cancer (IGROV), melanoma

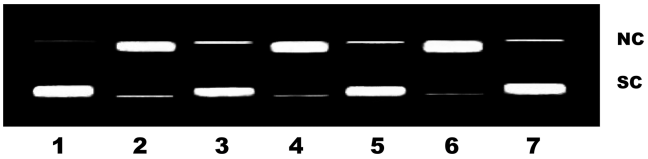

Figure 10. Analysis of the capacity of T4 DNA ligase to religate DNA cleaved by **1**−**3**. Lane 1, DNA control. Lane 2: products (NC ΦX174 RF) obtained from the reaction with complex **1**. Lane 3: lane 2 + T4 ligase. Lane 4: products (NC ΦX174 RF) obtained from the reaction with complex **2**. Lane 5: lane 4 + T4 ligase. Lane 6: products (NC ΦX174 RF) obtained from the reaction with complex **3**. Lane 7: lane 6 + T4 ligase.

(M19), and colon cancer (WIDR). For comparison, the cytotoxicities of six known anticancer drugs, viz., doxorubicin (DOX), cisplatin (CPT), 5-fluorouracil (5-FU), methotrexate (MTX), etoposide (ETO), and taxol (TAX), have also been screened against all of the above cell lines (Table 5). Indeed, a ligand or complex with an IC_{50} value higher than 10 μM is considered to be inactive.[77] The test results indicate that the free ligands $\mathbf{H(L^1)}$−$\mathbf{H(L^3)}$ are inactive (IC_{50}, 95 to >100 μM) to all of the cancer lines. However, chelation of free ligands with ruthenium(II) increases the cytotoxicities of the cancer cell lines. The cytotoxicities of **1**−**3** are insignificant for A498 and H226. Also, **1** shows low or no cytotoxicity at all in all of the cell lines except EVSA-T. The IC_{50} values obtained with **2** and **3** are higher compared to those achieved with CPT in IGROV, M19, MCF-7, and WIDR and with 5-FU in IGROV, M19, and WIDR. In all of the cell lines, the cytotoxicities of **2** and **3** are even higher than those reached with DOX, MTX, ETO, or TAX. Interestingly, **1**−**3** exhibit a similar potency against EVSA-T, which is comparable to CPT. The ability of the complexes to exhibit cytotoxicity follows the order **3** > **2** > **1** in all of the tested cell lines except EVSA-T. Earlier investigations have shown that the lower cationic charge of the complex and the hydrophobicity of the ligands confer greater lipophilicity, which promotes complex permeation across the cell membrane to exhibit cytotoxicity.[78] The monocationic charge of the complexes (**1**−**3**) and the hydrophobicity of the dangling pyridine rings of the coordinated ligands [$\mathbf{H(L^1)}$−$\mathbf{H(L^3)}$] might thus be attributed to the efficient cytotoxicity of complexes, in addition to their DNA and protein binding affinity. Further, the only structural difference among **1**−**3** is the substitution of electron-donating methyl group(s) in the 6 position [$\mathbf{H(L^2)}$ and **2**] and 4 and 6 positions [$\mathbf{H(L^3)}$ and **3**] of the dangling pyridine moiety of the Schiff-base ligand, and the increasing hydrophobicity follows the order dangling simple pyridine (**1**) < 6-methylpyridine (**2**) < 4,6-dimethylpyridine (**3**) (cf. above). A molecule with an elevated hydrophobicity also has an elevated lipophilicity (the lipophilicity is directly proportional to the hydrophobicity), which means it

https://doi.org/10.1021/acs.inorgchem.1c03399
Inorg. Chem. 2022, 61, 2864−2882

Table 5. *In Vitro* Cytotoxicity Assays for 1−3, DOX, CPT, 5-FU, MTX, ETO, and TAX Screened against Seven Human Tumor Cell Lines of Different Origins, viz., Renal Cancer (A498), Breast Cancer (EVSA-T and MCF7), Nonsmall Cell Lung Cancer (H226), Ovarian Cancer (IGROV), Melanoma (M19), and Colon Cancer (WIDR)

	drug[a] ($IC_{50}/\mu M$ Using SRB as the Cell Viability Test)								
cell line	1	2	3	DOX	CPT	5-FU	MTX	ETO	TAX
A498	50.811	48.510	42.520	0.166	7.509	1.099	0.081	1.803	<0.004
EVSA-T	2.913	2.514	1.810	0.015	1.406	3.651	0.011	0.435	<0.004
H226	32.400	19.913	15.823	0.366	10.895	2.613	5.033	5.397	<0.004
IGROV	16.601	8.699	7.010	0.110	0.563	2.283	0.015	0.780	<0.004
M19	10.020	5.599	4.110	0.029	1.860	3.397	0.051	0.693	<0.004
MCF7	10.905	5.701	4.412	0.018	2.330	5.764	0.040	3.551	<0.004
WIDR	14.523	8.020	5.701	0.020	3.223	1.729	<0.007	0.206	<0.004

[a]IC_{50} = concentration of the drug required to inhibit the growth of 50% of the cancer cells.

can permeate the cell membrane more easily. Therefore, the incorporation of methyl group(s) in the dangling pyridyl group enhances the cytotoxicity of the complex from **1** to **3**, and a subtle change in the ligand framework could contribute significantly to the cytotoxicity of the complex.

CONCLUSIONS

A new series of ruthenium(II) complexes of salicylaldimine-type ligands containing a dangling pyridine have been synthesized and characterized. The newly synthesized complexes (**1**−**3**) are obtained in the crystalline state, and thus the structures of the complexes $[Ru(bpy)_2(L^1/L^2/L^3)]^+$ possess a distorted octahedral geometry and exist as a dimer due to $\pi-\pi$-stacking and C−H···π interactions. They are involved in noncovalent interaction through the groove binding mode with DNA. DNA binding studies such as absorption, emission, CD spectral, and electrochemical studies suggest that **3** exhibits the highest binding affinity among the present complexes. It is noteworthy that these complexes show a higher propensity for binding to BSA protein in the hydrophobic region, which will be helpful to understand the drug−protein interaction. Remarkably, the ruthenium(II) complexes hydrolytically cleave SC DNA into NC and linear forms in the absence of any external reagent. Interestingly, they also show pH-dependent DNA damage, indicating that DNA is destroyed at the pH typical of hypoxic tumor cells, while little or no damage is identified at the pH distinctive of healthy cells. Such behavior is ascribed to the fact that (i) the dangling pyridine moiety can be protonated at low pH and the protonated form is the active agent or (ii) higher hydrophobicity encourages DNA binding and enhances the cleavage activity. All of the ruthenium(II) complexes involved in noncovalent DNA binding are cytotoxic to the human EVSA-T breast cancer cell line. Their cytotoxicity is comparable to CPT, which is presently used to treat breast cancer. Thus, the ruthenium(II) complexes of salicylaldimine-type ligands containing a dangling pyridine are new and improved DNA- and BSA-binding and DNA-cleaving agents and have the capability of being developed as effective cytotoxic drugs for the treatment of human breast cancer.

ASSOCIATED CONTENT

Supporting Information

The Supporting Information is available free of charge at https://pubs.acs.org/doi/10.1021/acs.inorgchem.1c03399.

Resonance Raman spectra, plots of [DNA] versus $[DNA]/(\varepsilon_a - \varepsilon_f)$, I_0/I versus [complex]/10^6, and i_{pc} versus $\nu^{1/2}$, CD spectra, differential pulse voltammograms, normal and modified Stern−Volmer plots of BSA, double-logarithmic plot of the quenching effect, absorption and fluorescence spectral properties, CD spectral parameters, and experimental details (PDF)

Accession Codes

CCDC 1567540, 1567542, and 1567544 contain the supplementary crystallographic data for this paper. These data can be obtained free of charge via www.ccdc.cam.ac.uk/data_request/cif, or by emailing data_request@ccdc.cam.ac.uk, or by contacting The Cambridge Crystallographic Data Centre, 12 Union Road, Cambridge CB2 1EZ, UK; fax: +44 1223 336033.

AUTHOR INFORMATION

Corresponding Author

Mariappan Murali − *Coordination and Bioinorganic Chemistry Research Laboratory, Department of Chemistry, National College (Autonomous), Tiruchirappalli 620001 Tamil Nadu, India;* orcid.org/0000-0001-8669-5939; Phone: +91-431-2482995; Email: murali@nct.ac.in, ma66mu@gmail.com; Fax: +91-431-2481997

Author

Somasundaram Sangeetha − *Coordination and Bioinorganic Chemistry Research Laboratory, Department of Chemistry, National College (Autonomous), Tiruchirappalli 620001 Tamil Nadu, India*

Complete contact information is available at: https://pubs.acs.org/10.1021/acs.inorgchem.1c03399

Notes

The authors declare no competing financial interest.

ACKNOWLEDGMENTS

We are grateful for the DST-FIST initiative of the National College (Autonomous), Tiruchirappalli, India. Thanks are due to STIC, Cochin University of Science and Technology, for the X-ray crystal structure data, and Dr. Babu Varghese, SAIF, Indian Institute of Technology Madras, for structure solution and refinement. The authors thank Professor A. Ramu, School of Chemistry, Madurai Kamaraj University, for CD spectral measurements. This paper is dedicated to Professor G. Mugesh, Department of Inorganic and Physical Chemistry, Indian Institute of Science, Bangalore, India for his magnificent contributions in the field of Chemical Biology, Bioinorganic and Medicinal Chemistry.

REFERENCES

(1) (a) Reedijk, J. Improved understanding in platinium antitumour chemistry. *Chem. Commun.* **1996**, 801−806. (b) Wong, E.; Giandomenico, C. M. Current status of platinum-based antitumor drugs. *Chem. Rev.* **1999**, *99*, 2451−2466.

(2) Reedijk, J. Why Does Cisplatin Reach Guanine-N7 with Competing S-Donor Ligands Available in the Cell? *Chem. Rev.* **1999**, *99*, 2499−2510.

(3) Brabec, V.; Kasparkova, J. Ruthenium coordination compounds of biological and biomedical significance. DNA binding agents. *Coord. Chem. Rev.* **2018**, *376*, 75−94.

(4) Allardyce, C. S.; Dyson, P. J. Ruthenium in Medicine: Current Clinical Uses and Future Prospects. *Platinum Met. Rev.* **2001**, *45*, 62−69.

(5) (a) Bratsos, I.; Jedner, S.; Gianferrara, T.; Alessio, E. Ruthenium Anticancer Compounds: Challenges and Expectations. *Chimia* **2007**, *61*, 692−697. (b) Alessio, E.; Mestroni, G.; Bergamo, A.; Sava, G. Ruthenium anticancer drugs. *Met. Ions Biol. Syst.* **2004**, *42*, 323−351. (c) Alessio, E.; Mestroni, G.; Bergamo, A.; Sava, G. Ruthenium antimetastatic agents. *Curr. Top. Med. Chem.* **2004**, *4*, 1525−1535. (d) Bacac, M.; Hotze, A. C. G.; van der Schilden, K.; Haasnoot, J. G.; Pacor, S.; Alessio, E.; Sava, G.; Reedijk, J. The hydrolysis of the anticancer ruthenium complex NAMI-A affects its DNA binding and antimetastatic activity: an NMR evaluation. *J. Inorg. Biochem.* **2004**, *98*, 402−412.

(6) (a) Jakupec, M. A.; Galanski, M.; Arion, V. B.; Hartinger, C. G.; Keppler, B. K. Antitumour metal compounds: more than theme and variations. *Dalton Trans.* **2008**, 183−194. (b) Hartinger, C. G.; Jakupec, M. A.; Zorbas- Seifried, S.; Groessl, M.; Egger, A.; Berger, W.; Zorbas, H.; Dyson, P. J.; Keppler, B. K. KP1019, a new redox-active anticancer agent–preclinical development and results of a clinical phase I study in tumor patients. *Chem. Biodiversity* **2008**, *5*, 2140−2155. (c) Hartinger, C. G.; Zorbas-Seifried, S.; Jakupec, M. A.; Kynast, B.; Zorbas, H.; Keppler, B. K. From bench to bedside-preclinical and early clinical development of the anticancer agent indazolium trans-tetrachlorobis(1H- indazole) ruthenate (III)] (KP1019 or FFC14A). *J. Inorg. Biochem.* **2006**, *100*, 891−904. (d) Jakupec, M. A.; Keppler, B. K. Gallium in cancer treatment. *Curr. Top. Med. Chem.* **2004**, *4*, 1575−1583.

(7) Alessio, E. Thirty Years of the Drug Candidate NAMI-A and the Myths in the Field of Ruthenium Anticancer Compounds: A Personal Perspective. *Eur. J. Inorg. Chem.* **2017**, *2017*, 1549−1560.

(8) Rilak Simovic, A.; Masnikosa, R.; Bratsos, I.; Alessio, E. Chemistry and reactivity of ruthenium(II) complexes: DNA/protein binding mode and anticancer activity are related to the complex structure. *Coord. Chem. Rev.* **2019**, *398*, 113011.

(9) Rosenberg, B.; Van Camp, L.; Trosko, J. E.; Mansour, V. H. Platinum compounds: a new class of potent antitumour agents. *Nature* **1969**, *222*, 385−386.

(10) Jiang, G. B.; Zhang, W. Y.; He, M.; Gu, Y.; Bai, L.; Wang, Y. J.; Yi, O.; Du, F. Development of Four Ruthenium Polypyridyl Complexes as Antitumor Agents: Design, Biological Evaluation and Mechanism Investigation. *J. Inorg. Biochem.* **2020**, *208*, 111104.

(11) Cini, R.; Defazio, S.; Tamasi, G.; Casolaro, M.; Messori, L.; Casini, A.; Morpurgo, M.; Hursthouse, M. Fac-$\{Ru(CO)_3\}^{2+}$-core complexes and design of metal-based drugs. synthesis, structure, and reactivity of Ru-thiazole derivative with serum proteins and absorption-release studies with acryloyl and silica hydrogels as carriers in physiological media. *Inorg. Chem.* **2007**, *46*, 79−92.

(12) (a) Dougan, S. J.; Sadler, P. J. The Design of Organometallic Ruthenium Arene Anticancer Agents. *Chimia* **2007**, *61*, 704−715. (b) Yan, Y. K.; Melchart, M.; Habtemariam, A.; Sadler, P. Organometallic chemistry, biology and medicine: ruthenium arene anticancer complexes. *J. Chem. Commun.* **2005**, 4764−4776. (c) Chen, H.; Parkinson, J. A.; Morris, R. E.; Sadler, P. J. Highly selective binding of organometallic ruthenium ethylenediamine complexes to nucleic acids: novel recognition mechanisms. *J. Am. Chem. Soc.* **2003**, *125*, 173−183.

(13) (a) Dyson, P. Systematic Design of a Targeted Organometallic Antitumour Drug in Pre- clinical Development. *Chimia J.* **2007**, *61*, 698−703. (b) Ang, W. H.; Dyson, P. J. Classical and Non-Classical Ruthenium-Based Anticancer Drugs: Towards Targeted Chemotherapy. *Eur. J. Inorg. Chem.* **2006**, *2006*, 4003−4018.

(14) Branden, C.; Tooze, J. *Introduction to Protein Structure*; Garland Publishing Inc., 1991.

(15) Martínez, R.; Chacón-García, L. The search of DNA-intercalators as antitumoral drugs: what it worked and what did not work. *Curr. Med. Chem.* **2005**, *12*, 127−151.

(16) Hannon, M. J. Supramolecular DNA recognition. *Chem. Soc. Rev.* **2007**, *36*, 280−295.

(17) Pindur, U.; Haber, M.; Sattler, K. Antitumor active drugs as intercalators of deoxyribonucleic acid: Molecular models of intercalation complexes. *J. Chem. Educ.* **1993**, *70*, 263−272.

(18) (a) Barton, J. K. Metals and DNA: molecular left-handed complements. *Science* **1986**, *233*, 727−734. (b) Xiong, Y.; Ji, L.-N. Synthesis, DNA-binding and DNA-mediated luminescence quenching of Ru(II) polypyridine complexes. *Coord. Chem. Rev.* **1999**, *185-186*, 711−733.

(19) (a) Rajendiran, V.; Murali, M.; Suresh, E.; Sinha, S.; Somasundaram, K.; Palaniandavar, M. Mixed ligand ruthenium(II) complexes of bis(pyrid-2-yl)-/bis(benzimidazol-2-yl)- dithioether and diimines: study of non-covalent DNA binding and cytotoxicity. *Dalton Trans.* **2008**, 148−163. (b) Rajendiran, V.; Murali, M.; Suresh, E.; Palaniandavar, M.; Periasamy, V. S.; Akbarsha, M. A. Non-covalent DNA binding and cytotoxicity of certain mixed-ligand ruthenium(II) complexes of 2,2′-dipyridylamine and diimines. *Dalton Trans.* **2008**, 2157−2170.

(20) (a) Dervan, P. B.; Burli, R. W. Sequence-specific DNA recognition by polyamides. *Curr. Opin Chem. Biol.* **1999**, *3*, 688−693. (b) Liu, J.-G.; Ye, B.-H.; Li, H.; Zhen, Q.-X.; Ji, L. - N.; Fu, Y.-H. Polypyridyl ruthenium(II) complexes containing intramolecular hydrogen- bond ligand: syntheses, characterization, and DNA-binding properties. *J. Inorg. Biochem.* **1999**, *76*, 265−271. (c) Maheswari, P. U.; Palaniandavar, M. DNA binding and cleavage properties of certain tetrammine ruthenium(II) complexes of modified 1,10- phenanthrolines-effect of hydrogen-bonding on DNA-binding affinity. *J. Inorg. Biochem.* **2004**, *98*, 219−230. (d) Caspar, R.; Musatkina, L.; Tatosyan, A.; Amouri, H.; Gruselle, M.; Guyard-Duhayon, C.; Duval, R.; Cordier, C. Efficient DNA binding by optically Pure Ruthenium Tris(bipyridyl) complexes incorporating carboxylic functionalities. Solution and structural analysis. *Inorg. Chem.* **2004**, *43*, 7986−7993.

(21) Paul, B. K.; Samanta, A.; Guchhait, N. Exploring hydrophobic subdomain IIA of the protein bovine serum albumin in the native, intermediate, unfolded, and refolded states by a small fluorescence molecular reporter. *J. Phys. Chem. B* **2010**, *114*, 6183−6196.

(22) Zhang, G.; Keita, B.; Brochon, J. C.; de Oliveira, P.; Nadjo, L.; Craescu, C. T.; Miron, S. Molecular interaction and energy transfer between human serum albumin and polyoxometalates. *J. Phys. Chem. B* **2007**, *111*, 1809−1814.

(23) Mohanraj, M.; Ayyannan, G.; Raja, G.; Jayabalakrishnan, G. Evaluation of DNA binding, DNA cleavage, protein binding, radical scavenging and in vitro cytotoxic activities of ruthenium(II) complexes containing 2,4-dihydroxy benzylidene ligands. *Mater. Sci. Eng. C* **2016**, *69*, 1297−1306.

(24) Lázaro, E.; Lowe, P. J.; Briand, X.; Faller, B. New approach to measure protein binding based on a parallel artificial membrane assay and human serum albumin. *J. Med. Chem.* **2008**, *51*, 2009−2017.

(25) Maheswari, P. U.; Roy, S.; den Dulk, H.; Barends, S.; van Wezel, G.; Kozlevcar, B.; Gamez, P.; Reedijk, J. The square-planar cytotoxic [Cu(II)(pyrimol)Cl] complex acts as an efficient DNA cleaver without reductant. *J. Am. Chem. Soc.* **2006**, *128*, 710−711.

(26) Maheswari, P. U.; Barends, S.; Özalp-Yaman, S.; de Hoog, P.; Casellas, H.; Teat, S. J.; Massera, C.; Lutz, M.; Spek, A. L.; van Wezel, G. P.; Gamez, P.; Reedijk, J. Unique ligand-based oxidative DNA cleavage by zinc(II) complexes of hpyramol and hpyrimol. *Chem. Eur. J.* **2007**, *13*, 5213−5222.

https://doi.org/10.1021/acs.inorgchem.1c03399
Inorg. Chem. 2022, 61, 2864−2882

(27) Sullivan, B. P.; Salmon, D. J.; Meyer, T. J. Mixed phosphine 2,2′-bipyridine complexes of ruthenium. *Inorg. Chem.* **1978**, *17*, 3334−3341.
(28) Boyd, M. R. In *Cancer: Principles and Practice of Oncology Update*; De Vita, V. T., Jr., Hellman, S., Rosenberg, S. A., Eds.; Lippincott: Philadelphia, PA, 1989; Vol. *3*, pp 1−12.
(29) Walker, N.; Stuart, D. An empirical method for correcting diffractometer data for absorption effects. *Acta Crystallogr.* **1983**, *39*, 158−166.
(30) Altomare, A.; Burla, M. C.; Camalli, M.; Cascarano, G. L.; Giacovazzo, C.; Guagliardi, A.; Moliterni, A. G. G.; Polidori, G.; Spagna, R. A new tool for crystal structure determination and refinement. *J. Appl. Crystallogr.* **1999**, *32*, 115−119.
(31) Sheldrick, G. M. *SHELX-97: Program for Refinement of Crystal Structure*; University of Göttingen: Göttingen, Germany, 1997.
(32) Marmur, J. A procedure for the isolation of deoxyribonucleic acid from micro-organisms. *J. Mol. Biol.* **1961**, *3*, 208−218.
(33) Sulkowska, A.; Równicka, J.; Bojko, B.; Sułkowski, W. J. Interaction of anticancer drugs with human and bovine serum albumin. *J. Mol. Struct.* **2003**, *651*, 133−140.
(34) Keepers, Y. P.; Pizao, P. E.; Peters, G. J.; van Ark-Otte, J.; Winograd, B.; Pinedo, H. M. Comparison of the sulforhodamine B protein and tetrazolium (MTT) assays for in vitro chemosensitivity testing. *Eur. J. Cancer Clin. On.* **1991**, *27*, 897−900.
(35) Flett, M. St. C. Studies of the band near 3 μ in some hydroxy compounds. *Spectrochim. Acta* **1957**, *10*, 21−37.
(36) Choudhury, S.; Kakoti, M.; Deb, A. K.; Goswami, S. Isomeric complexes of ruthenium(II) with neutral heterocyclic schiff base ligands. High resolution proton resonance spectra of *trans-cis* isomeric pairs of RuX_2L_2 and comparison of their physical properties. *Polyhedron* **1992**, *11*, 3183−3190.
(37) Evans, D. F.; Jakubovic, D. A. Complexes of a water-soluble tridentate schiff base ligand with a number of "hard" metal ions. *Polyhedron* **1988**, *7*, 2723−2726.
(38) Rillema, D. P.; Jones, D. S. Structure of tris(2,2′-bipyridyl)-ruthenium(II) hexafluorophosphate, $[Ru(bipy)_3][PF_6]_2$; *X*-ray crystallographic determination. *J. Chem. Soc., Chem. Commun.* **1979**, 849−851.
(39) Chakraborty, S.; Walawalkar, M. G.; Lahiri, G. K. Ruthenium-(II)/(III) pyridine heterochelates incorporating phenolato imine functionalities. Synthesis, crystal structure, spectroscopic and electron-transfer properties and solution reactivities. *J. Chem. Soc., Dalton Trans.* **2000**, 2875−2883.
(40) Bag, N.; Choudhury, S. B.; Pramanik, A.; Lahiri, G. K.; Chakravorty, A. Ruthenium(II) phenolates. Synthesis and characterization of a novel four-membered metallacycle. *Inorg. Chem.* **1990**, *29*, 5013−5014.
(41) Moustakali-Mavridis, I.; Hadjoudis, E.; Mavridis, A. Crystal and molecular structure of some thermochromic Schiff bases. *Acta Crystallogr.* **1978**, *B34*, 3709−3715.
(42) Hunter, C. A.; Sanders, J. K. M. The nature of. pi.-.pi. interactions. *J. Am. Chem. Soc.* **1990**, *112*, 5525−5534.
(43) Moustakalimavridis, I.; Hadjoudis, E.; Mavridis, A. Structure of thermochromic Schiff bases. II. Structures of N-salicylidene-3-aminopyridine and N-(5-methoxysalicylidene)-3- aminopyridine. *Acta Crystallogr., Sect. B: Struct. Sci.* **1980**, *36*, 1126−1130.
(44) (a) Pankuch, B. J.; Lacky, D. E.; Crosby, G. A. Charge-transfer excited states of osmium(II) complexes. 1. Assignment of the visible absorption bands. *J. Phys. Chem.* **1980**, *84*, 2061−2067. (b) Ceulemans, A.; Vanquickenborne, L. G. Charge-transfer spectra of iron(II)- and ruthenium(II)-tris(2,2′-bipyridyl) complexes. *J. Am. Chem. Soc.* **1981**, *103*, 2238−2241. (c) Decurtins, S.; Felix, F.; Ferguson, J.; Gudel, H. U.; Ludi, A. The electronic spectrum of tris(2,2′-bipyridine)iron(2+) and tris (2,2′-bipyridine) osmium(2+). *J. Am. Chem. Soc.* **1980**, *102*, 4102−4106. (d) Kober, E. M.; Meyer, T. J. Concerning the absorption spectra of the ions $M(bpy)_3^{2+}$ (M = Fe, Ru, Os; bpy = 2,2′-bipyridine). *Inorg. Chem.* **1982**, *21*, 3967−3977.
(45) (a) Coe, B. J.; Meyer, T. J.; White, P. S. Synthetic and Structural Studies on trans- Tetrapyridine Complexes of Ruthenium-(II). *Inorg. Chem.* **1995**, *34*, 593−602. (b) Paw, W.; Connick, W. B.; Eisenberg, R. Dipyridocatecholate-Bridged Complexes of Platinum and Ruthenium Diimine Chromophores. *Inorg. Chem.* **1998**, *37*, 3919−3926. (c) Alsfasser, R.; van Eldik, R. Novel Building Blocks for Biomimetic Assemblies. Synthesis, Characterization, and Spectroscopic and Electrochemical Properties of New Bidentate Ligands Derived from Lysine and Cysteine and Their Complexes with Bis(2,2′-bipyridine)ruthenium(II). *Inorg. Chem.* **1996**, *35*, 628−636.
(46) (a) Mayoh, B.; Day, P. The excited states of bipyridyl and phenanthroline complexes of Fe(III), Ru(II) and Ru(III) A molecular orbital study. *Theor. Chim. Acta J. Am. Chem. Soc.* **1978**, *49*, 259−275. Orgel, L. E. Double bonding in chelated metal complexes. *J. Chem. Soc.* **1961**, 3683−3686.
(47) Holligan, B. M.; Jeffery, J. C.; Norgett, M. K.; Schatz, E.; Ward, M. D. The co-ordination chemistry of mixed pyridine−phenol ligands; spectroscopic and redox properties of mononuclear ruthenium complexes with $(pyridine)_{6-x}(phenolate)_x$ donor sets (x = 1 or 2). *Chem. Soc., Dalton Trans.* **1992**, 3345−3351.
(48) Brown, G. M.; Weaver, T. R.; Keene, F. R.; Meyer, T. J.; Kenan, W. R. Oxidation of coordinated diamines in bis(2,2′-bipyridine) complexes of ruthenium. *Inorg. Chem.* **1976**, *15*, 190−196.
(49) Callahan, R. W.; Keene, F. R.; Meyer, T. J.; Salmon, D. J. Intervalence transfer and electron transfer in the mixed-valence ion dichlorotetrakis(bipyridine)pyrazineruthenium (3+). *J. Am. Chem. Soc.* **1977**, *99*, 1064−1073.
(50) (a) Bag, N.; Lahiri, G. K.; Bhattacharya, S.; Falvello, L. R.; Chakravorty, A. Ruthenium Phenolates. Chemistry of a family of RuIIIO6 tris chelates. *Inorg. Chem.* **1988**, *27*, 4396−4402. (b) Lahiri, G. K.; Bhattacharya, S.; Goswami, S.; Chakravorty, A. High- potential isomeric ruthenium(III) complexes of 2-(phenylazo)pyridine. *J. Chem. Soc., Dalton Trans.* **1990**, 561−565.
(51) Rillema, D. P.; Jones, D. S.; Woods, C.; Levy, H. A. Comparison of the crystal structures of tris heterocyclic ligand complexes of ruthenium(II). *Inorg. Chem.* **1992**, *31*, 2935−2938.
(52) Strekas, T. C.; Gafney, H. D.; Tysoe, S. A.; Thummel, R. P.; Lefoulon, F. Resonance Raman spectra and excited-state lifetimes for a series of 3,3′-polymethylene-2,2′-bipyridine complexes of ruthenium(II). *Inorg. Chem.* **1989**, *28*, 2964−2967.
(53) Strommen, D. P.; Mallick, P. K.; Danzer, G. D.; Lumpkin, R. S.; Kincaid, H. J. R. Normal- coordinate analyses of the ground and 3MLCT excited states of tris(bipyridine)ruthenium (II). *J. Phys. Chem.* **1990**, *94*, 1357−1366.
(54) Keyes, T. K.; Leane, D.; Forster, R. J.; Coates, C. G.; McGarvey, J. J.; Nieuwenhuyzen, M. N.; Figgemeier, E.; Vos, J. G. Redox and Spectroscopic Orbitals in Ru(II) and Os(II) Phenolate Complexes. *Inorg. Chem.* **2002**, *41*, 5721−5732.
(55) Keyes, T. E.; Jayaweera, P. M.; McGarvey, J. J.; Vos, J. G. Electronic properties of hydroquinone-containing ruthenium complexes in different oxidation states. *J. Chem. Soc., Dalton Trans.* **1997**, 1627−1632.
(56) Maikoo, S.; Kirkpatrick Dingle, L. M.; Chakraborty, A.; Xulu, B.; Edkins, A. L.; Booysen, I. N. Synthetic, characterization and cytotoxic studies of ruthenium complexes with Schiff bases encompassing biologically relevant moieties. *Polyhedron.* **2020**, *184*, 114569.
(57) Rajarajeswari, C.; Loganathan, R.; Palaniandavar, M.; Suresh, E.; Riyasdeen, A.; Akbarsha, M. A. Copper(II) complexes with 2NO and 3N donor ligands: synthesis, structures and chemical nuclease and anticancer activities. *Dalton Trans.* **2013**, *42*, 8347−8363.
(58) Zhang, Z.; Yang, Z.; Wu, Y.; Yuan, Z.; Du, J.; Li, L. Reduced amino acid Schiff base containing ruthenium(III) complexes: Synthesis, characterization, DNA interaction, and in vitro Cytotoxicity. *J. Biochem. Mol. Toxicol.* **2020**, *34*, No. e22510.
(59) Paul, H.; Mukherjee, T.; Drew, M. G. B.; Chattopadhyay, P. Synthesis, characterization, crystal structure, and DNA-binding of ruthenium(II) complexes of heterocyclic nitrogen ligands resulting from a benzimidazole-based quinazoline derivative. *J. Coord. Chem.* **2012**, *65*, 1289−1302.

https://doi.org/10.1021/acs.inorgchem.1c03399
Inorg. Chem. 2022, 61, 2864−2882

(60) Lakowicz, J. R.; Weber, G. Quenching of fluorescence by oxygen. A probe for structural fluctuations in macromolecules. *Biochemistry* **1973**, *12*, 4161−4170.
(61) Ganeshpandian, M.; Loganathan, R.; Suresh, E.; Riyasdeen, A.; Akbarsha, M. A.; Palaniandavar, M. New ruthenium(II) arene complexes of anthracenyl-appended diazacycloalkanes: effect of ligand intercalation and hydrophobicity on DNA and protein binding and cleavage and cytotoxicity. *Dalton Trans.* **2014**, *43*, 1203−1219.
(62) Richter, S.; Singh, S.; Draca, D.; Kate, A.; Kumbhar, A.; Kumbhar, A. S.; Maksimovic- Ivanic, D.; Mijatovic, S.; Lönnecke, P.; Hey-Hawkins, E. Antiproliferative activity of ruthenium(II) arene complexes with mono- and bidentate pyridine-based ligands. *Dalton Trans.* **2016**, *45*, 13114−13125.
(63) Johnston, D. H.; Cheng, C.-C.; Campbell, K. J.; Thorp, H. H. Trans-Dioxorhenium(V)- Mediated Electrocatalytic Oxidation of DNA at Indium Tin-Oxide Electrodes: Voltammetric Detection of DNA Cleavage in Solution. *Inorg. Chem.* **1994**, *33*, 6388−6390.
(64) Mahadevan, S.; Palaniandavar, M. Spectral and Electrochemical Behavior of Copper(II)- Phenanthrolines Bound to Calf Thymus DNA. [(5,6-dimethyl-OP)(2)Cu](2+) (5,6- dimethyl- OP = 5,6-Dimethyl-1,10-phenanthroline) Induces a Conformational Transition from B to Z DNA. *Inorg. Chem.* **1998**, *37*, 3927−3934.
(65) Lakowicz, J. R. *Principles of Fluorescence Spectroscopy*, 3rd ed.; Springer Science + Business Media: New York, 2006.
(66) Eftink, M. R.; Ghiron, C. A. Fluorescence quenching of indole and model micelle systems. *J. Phys. Chem.* **1976**, *80*, 486−493.
(67) Zhao, X.; Liu, R.; Chi, Z.; Teng, Y.; Qin, Y. New insights into the behavior of bovine serum albumin adsorbed onto carbon nanotubes: comprehensive spectroscopic studies. *J. Phys. Chem. B* **2010**, *114*, 5625−5631.
(68) Zhang, X.; Li, S.; Yang, L.; Fan, C. Synthesis, characterization of Ag(I), Pd(II) and Pt(II) complexes of a triazine-3-thione and their interactions with bovine serum albumin. *Spectrochim. Acta Part A Mol. Biomol. Spectrosc.* **2007**, *68*, 763−770.
(69) Devagi, G.; Dallemer, F.; Kalaivani, P.; Prabhakaran, R. Organometallic ruthenium(II) complexes containing NS donor Schiff bases: Synthesis, structure, electrochemistry, DNA/BSA binding, DNA cleavage, radical scavenging and antibacterial activities. *J. Organomet. Chem.* **2018**, *854*, 1−14.
(70) Lehrer, S. S. Solute perturbation of protein fluorescence. The quenching of the tryptophyl fluorescence of model compounds and of lysozyme by iodide ion. *Biochemistry* **1971**, *10*, 3254−3263.
(71) Anuja, P. K.; Paira, P. Luminescent anticancer Ru(II)-arenebipyridine and phenanthroline complexes: Synthesis, characterization, DFT studies, biological interactions and cellular imaging application. *J. Inorg. Biochem.* **2020**, *208*, 111099.
(72) Ahmad, B.; Parveen, S.; Khan, R. H. Effect of albumin conformation on the binding of ciprofloxacin to human serum albumin: a novel approach directly assigning binding site. *Biomacromolecules* **2006**, *7*, 1350−1356.
(73) Zhang, G.; Chen, X.; Guo, J.; Wang, J. Spectroscopic investigation of the interaction between chrysin and bovine serum albumin. *J. Mol. Struct.* **2009**, *921*, 346−351.
(74) Kamatchi, T. S.; Kalaivani, P.; Fronczek, F. R.; Natarajan, K.; Prabhakaran, R. Impact of chelation on anticancer activities of organometallic ruthenium(II) complexes containing 2,5-di(1*H*-pyrazol-1-yl)-1,4-benzoquinone: Synthesis, structure, DNA/protein binding, antioxidant activity and Cytotoxicity. *RSC Adv.* **2016**, *6*, 46531−46547.
(75) Tayeh, N.; Rungassamy, T.; Albani, J. R. Fluorescence spectral resolution of tryptophan residues in bovine and human serum albumins. *J. Pharm. Biomed. Anal.* **2009**, *50*, 107−116.
(76) (a) Pamatong, F. V.; Detmer, C. A., III; Bocarsly, J. R. Double-Strand Cleavage of DNA by a Monofunctional Transition Metal Cleavage Agent. *J. Am. Chem. Soc.* **1996**, *118*, 5339−5345. (b) Detmer, C. A., III; Pamatong, V.; Bocarsly, J. R. Nonrandom Double Strand Cleavage of DNA by a Monofunctional Metal Complex: Mechanistic Studies. *Inorg. Chem.* **1996**, *35*, 6292−6298.
(77) Ingrassia, L.; Nshimyumukiza, P.; Dewelle, J.; Lefranc, F.; Wlodarczak, L.; Thomas, S.; Dielie, G.; Chiron, C.; Zedde, C.; Tisnes, P.; van Soest, R.; Braekman, J. C.; Darro, F.; Kiss, R. A lactosylated steroid contributes in vivo therapeutic benefits in experimental models of mouse lymphoma and human glioblastoma. *J. Med. Chem.* **2006**, *49*, 1800−1807.
(78) Schluga, P.; Hartinger, C. G.; Egger, A.; Reisner, E.; Galanski, M.; Jakupec, M. A.; Keppler, B. K. Redox behavior of tumor-inhibiting ruthenium(III) complexes and effects of physiological reductants on their binding to GMP. *Dalton Trans.* **2006**, 1796−1802.

NOTE ADDED AFTER ASAP PUBLICATION

This paper was published on January 31, 2022. Due to production error, an incorrect version of Figure 4 was included. The corrected version was reposted on February 2, 2022.

https://doi.org/10.1021/acs.inorgchem.1c03399
Inorg. Chem. 2022, 61, 2864−2882